Review

Status and Perspectives of Continuous Gravitational Wave Searches

Ornella Juliana Piccinni [1,2]

1   INFN, Sezione di Roma, I-00185 Roma, Italy; ornella.juliana.piccinni@roma1.infn.it or opiccinni@ifae.es
2   Institut de Física d'Altes Energies (IFAE), Barcelona Institute of Science and Technology, and ICREA, E-08193 Barcelona, Spain

Abstract: The birth of gravitational wave astronomy was triggered by the first detection of a signal produced by the merger of two compact objects (also known as a compact binary coalescence event). The following detections made by the Earth-based network of advanced interferometers had a significant impact in many fields of science: astrophysics, cosmology, nuclear physics and fundamental physics. However, compact binary coalescence signals are not the only type of gravitational waves potentially detectable by LIGO, Virgo, and KAGRA. An interesting family of still undetected signals, and the ones that are considered in this review, are the so-called continuous waves, paradigmatically exemplified by the gravitational radiation emitted by galactic, fast-spinning isolated neutron stars with a certain degree of asymmetry in their mass distribution. In this work, I will review the status and the latest results from the analyses of advanced detector data.

Keywords: continuous gravitational waves; neutron stars; dark matter; LIGO; Virgo; KAGRA

1. Introduction

To date, the LIGO and Virgo interferometric detectors [1–3] have registered 90 gravitational wave (GW) events from the coalescence and merger of two compact bodies, either a pair of black holes (BHs) or neutron stars (NSs) or a mixed NS–BH system [4–7]. Each confirmed detection, starting from the first event in September 2015, has added a big piece of information about our comprehension of nature. However, there is still a huge pile of missing pieces to be added to the puzzle before having a complete picture of the GW sky. Indeed, the GW community is only at the beginning of the newborn GW astronomy. Gathering all the information collected so far, GW scientists have been able to prove, among other things, the existence of GWs, the possibility of having BHs in binaries, and the formation of heavy elements in NSs mergers, etc., just by considering the class of transient GW events. In principle, the number of potentially emitting sources is really large, since any system is able to generate GWs whenever there is a non-vanishing mass quadrupole moment. In particular, other astrophysical systems are able to emit GWs potentially detectable by Earth-based interferometers such as LIGO, Virgo and KAGRA [1,2,8]. In this review, I will focus on the discussion of the prospects of detection for a particular subset of GW signals called continuous waves (CWs). Although the emitted signal in this case might be difficult to catch in the data, a detection would certainly be of wide interest to the full scientific community. In Section 2, I will provide some information about the physical systems that can emit CWs signals. In Section 3, I will provide an up-to-date discussion of the data analysis techniques used for this type of problem. Finally, in Section 4, I will report the latest observational results, while conclusions are given in Section 5.

2. Sources of Continuous GWs

The detection of continuous GW signals represents one of the next milestones to reach in gravitational-wave astronomy. Long-lasting signals, persistent over the full observing run (i.e., the data taking period), or in its shorter duration version, the so-called long CW

transients, are typically emitted by fast spinning asymmetric NSs, both in accreting systems or as isolated sources. To this canonical set of sources, recent studies have reported the possibility of also observing the continuous gravitational emission by potential dark matter (DM) candidates. Other potential sources of CWs are boson stars [9,10] and Thorne-Żytkow Objects [11], although no associated search in advanced detector data has been carried out yet.

In this section, I will review the main emission models proposed in the literature. Previous reviews about CW signals and searches can be found in [12–17] or in the more general GW reviews [18,19].

2.1. Neutron Stars

The physical condition of NS matter is unique, making these fascinating compact objects precious laboratories for subatomic and fundamental physics [20,21]. High density and pressure are reached as the inner core is approached, with an average density comparable with terrestrial atomic nuclei ($\rho_0 \sim 2.5 \times 10^{14}$ g/cm^3), up to values one order of magnitude bigger in the inner core. Surface magnetic fields can reach values up to 10^{12} Gauss or 10^{15} Gauss for strongly magnetized NSs, also known as magnetars [22,23]. Given the extreme condition of NS matter, the equation of state (EOS) is not completely known since superfluidity, superconductivity [24,25], exotic states or quantum effects might be present [26–29]. The actual NS composition is still unknown. In particular, when higher densities are reached, the hadronic nuclear matter undergoes a de-confinement transition to a new phase of quarks and gluons [30], although how this phase transition occurs is still unclear. In a different scenario, the NS inner core can be composed of hyperons [31], Bose–Einstein, pion or kaon condensates [32–34] and more. Furthermore, some of the above-mentioned states of matter can be simultaneously present inside the compact object. The NS matter EOS directly reflects on the star's observable global parameters such as the mass and the radius. Theoretical and observational efforts, including those related to GWs, to measure the NS masses and radii are ongoing [35–39]. To set constraints on the EOS of isolated NSs, both mass and radius should be measured, and some assumptions on the pulse profiles should be made (see, e.g., [40]). NS masses are typically measured from pulsar observations, while radius measurements are more challenging and strongly depend on the X-ray emission model assumed. To date, the NS measured masses lie in the range $[1.1; 2.2]$ $M_\odot$, with the most massive source being the millisecond pulsar J0740+6620 with a mass of 2.14 $M_\odot$ [41]. Direct measurements of radii do not exist; however, estimates can be made, for instance, by combining the measured flux and temperature with the source distance. Current estimates report NS radii in the range $[9; 13]$ km [42–44]. Further improvements on the NS radius and mass estimates are provided by the NICER mission [45,46]. The detection of the first NS merger event GW170817 by LIGO and Virgo [47], followed by the electromagnetic (EM) gamma-ray burst GRB170817 [48], and the optical transient signal of a kilonova (AT 2017gfo) [49], provided a new tool for NS mass and radius estimates [50], extending the possible NS mass range. Other GW events involving potential NS have been reported to date: GW190425 [51] with a progenitor mass of $[1.12; 2.52]$ $M_\odot$ and GW190814 [52] involving a compact object with a mass of $2.50 - 2.67$ $M_\odot$. No EM counterpart has been observed from the two events, suggesting that these are the smallest BHs to date, although the possibility of being the most massive NSs measured so far cannot be completely excluded. To this list of GW signals involving at least a (potential) NS, there are the events: GW190917_114630 [6], GW191219_163120 [7], GW200210_092254 [7] and the two GW200105_162426 and GW200115_042309 discussed in [7,53].

The formation of an NS could happen through two main channels: (i) core-collapse supernova explosions (CCSN), forming a very hot proto-neutron star, followed by a cooler stable NS [54], (ii) after a binary NS merger [55]. In these two scenarios, fast-rotating and highly magnetized young NS (in particular magnetars) could be formed.

Spinning NSs are expected to emit GWs continuously if they are asymmetric with respect to their rotation axis [56,57]. Potential targets for Earth-based detectors are galactic

sources. The signal produced as the star spins is almost monochromatic and with a frequency proportional to the star's spin frequency. Four different scenarios are considered possible for the observation of CWs, namely (i) very hot newborn NSs, right after the formation, i.e., after merger and core-collapse supernova, reaching rotating frequencies close to their Keplerian limit; (ii) young NSs such as stable supernova remnants during the initial spin-down phase; (iii) accreting low mass X-ray binaries (LMXBs) emitting thermal X-ray radiation and characterized by a small spin-up; (iv) fast-spinning pulsars, i.e., old millisecond pulsars with small spin-down. Different CW emission models are considered (see [56]), and these include the emission due to the presence of non-axisymetries in rigid rotating triaxial bodies, rotating about one of its principal axes (equivalent to a biaxial rotor not spinning about one of the principal axes); oscillation of the star; or more complicated scenarios such as free precessing systems or heterogeneous stars (when multiple phases of component matter are simultaneously present, including superfluidity).

If from one side, some of the GW emission mechanisms are well understood, the actual factors that cause the asymmetry in the star are still under debate. Indeed, the asymmetry could be triggered by the presence of residual crustal deformations (e.g., after a fast cooling of the NS crust), the presence of a strong inner magnetic field not aligned with the star's rotation axis, or the presence of magnetic or thermal "mountains" (see [17] for a review). The maximum ellipticity (i.e., deformability) the star can sustain depends on both the NS EOS and the breaking strain of the crust [15]. I briefly review the two main CW emission mechanisms happening in NSs and how these reflect on the expected signal amplitude.

Ellipticity driven emission: the GW amplitude for an NS with asymmetries can be expressed in terms of the product between the moment of inertia I_3 along the spin axis and the star's degree of asymmetry, also known as ellipticity ε:

$$h_0 = \frac{16\pi^2 G}{c^4} \frac{I_3 \varepsilon f_{\mathrm{spin}}^2}{r} \tag{1}$$

where f_{spin} is the star spin frequency of a source at a distance r. Most of the observed NSs have rotation frequencies below 1 kHz, i.e., in the sensitivity range of ground-based interferometers such as advanced LIGO/Virgo. The ellipticity is given by $\varepsilon = \frac{I_2 - I_1}{I_3}$, assuming $I_1 \neq I_2$. Most of the parameters entering in Equation (1) can be somehow constrained by astronomical observations, except for the ellipticity ε for which only theoretical maxima estimates exist [58–63]. Current estimates only report upper limits in the 10^{-7}–10^{-5} range, while an actual estimate of a fiducial ellipticity of $\sim 10^{-9}$, possibly sustained by millisecond pulsars, is given in [61].

For the case of elastic stresses, the maximum sustainable ellipticity is related to the crustal breaking strain u_{break} as [64]

$$\varepsilon < 2 \times 10^{-5} \left(\frac{u_{\mathrm{break}}}{0.1} \right) \tag{2}$$

with estimated values of $u_{\mathrm{break}} = 0.1$, much larger than standard terrestrial materials [65]. However, these constraints strongly depend on the actual EOS (see, e.g., [15]).

For quadrupolar deformations on spherically symmetric stars due to magnetic fields [66–68], the ellipticity is given by the ratio of the magnetic energy and the GW energy. The actual deformation strongly depends on the magnetic field morphology. Indeed, poloidal fields will oblate the star, while toroidal fields tend to prolate the star. When the magnetic field is purely poloidal, the ellipticity will depend on the average $\bar{B}$ field as

$$\varepsilon \approx 10^{-12} \left(\frac{\bar{B}}{10^{12}\mathrm{G}} \right)^2 . \tag{3}$$

In the case of a fully toroidal magnetic field, the star's ellipticity is given by

$$\varepsilon \approx 10^{-11} \left(\frac{\bar{B}}{10^{12}\text{G}} \right)^2.$$ (4)

In a realistic scenario, also known as "twisted-torus" configuration, both the poloidal and toroidal components will contribute to the B field (for a detailed discussion, see [15,17,56]). Given the uncertainty connected to the estimation of ε and the moment of inertia I, typically the deviation from axisymmetry is constrained in terms of the quadrupole Q_{22} (assuming that the $l = m = 2$ mode dominates) [59]

$$Q_{22} = \sqrt{\frac{8\pi}{15}} \varepsilon I.$$ (5)

R-mode emission: a different emission channel for CW radiation is given by the Rossby (r-)modes oscillations in rotating stars. R-mode emission is provided by the Chandrasekhar–Friedman–Schutz instability, leading to the rapid growth of the r-mode amplitude until a saturation amplitude is reached and the growth of the mode stops [69]. These amplitudes are damped by the viscosity of the star. Given these two opposite effects, where the amplitude increases with the spin of the star and is suppressed by the viscosity, dependent on the temperature, an instability window is defined in the angular velocity-temperature plane [70]. Typically, NSs are unstable to r-modes except at extreme temperatures. At very low temperatures, the shear viscosity dominates the damping, while at very high temperatures, the bulk viscosity takes the lead in the r-mode suppression. Given this strict relation with the inner physics of the NS during the r-mode emission, constraints on the GW observable properties are interesting tools for the study of the EOS [56,71]. A typical parameter constrained in CW searches for r-modes is the r-mode amplitude α. Considering a source at a distance r the GW strain h_0 is given by [72]:

$$h_0 = \sqrt{\frac{2^9 \pi^7}{5} \frac{G}{c^5} \tilde{J} M R^3 \frac{f_{\text{gw}}^3 \alpha}{r}}$$ (6)

where the dimensionless constant $\tilde{J}$ is connected to the source density and EOS [69,72]. M and R are the NS mass and radius. The GW frequency f_{gw} is proportional to the oscillation angular frequency $\omega = 2\pi f_{\text{gw}}$, which is related to the rotation angular velocity as $\omega \sim -4\Omega/3$. If relativistic corrections and other effects due to the rotation are considered [73, 74], e.g., those related to the EOS, the relation between the GW frequency and the star spin frequency can be parametrized as [74,75]:

$$f_{\text{gw}} = A f_{\text{spin}} + B \left(\frac{f_{\text{spin}}}{f_{\text{Kepler}}} \right)^2 f_{\text{spin}}$$ (7)

where f_{Kepler} is the Kepler frequency of the star, i.e., its maximum sustainable spin frequency. The values for A and B lie in a range $1.39 < A < 1.57$ and $0 < B < 0.195$.

Ellipticities are also expected to be present in LMXBs, due to an asymmetric accretion process, producing, for instance, thermal gradients in the crust [58]. In these systems, a spinning NS is accreting matter from a companion, forming a circumstellar accretion disk around it and emitting strong X-ray radiation. These systems represent interesting targets for CW searches [76] given that when the accretion torque balances the GW torque, LMXBs become very stable GW emitters. In particular, the GW amplitude of an LMXBs is proportional to the square root of the X-ray flux. For this reason, very bright sources such as Scorpius X-1 (Sco X-1) or XTE J1751-305 represent ideal targets. It has been observed that all the NSs in LMXB systems have maximum spinning frequencies below their Keplerian breakup limit. Indeed, the fastest LMXB observed has a spin frequency of $\sim$700 Hz, while according to [77], the lowest breakup frequency allowed is $\sim$1200 Hz, although this limit

strongly depends on the assumptions made for the EOS of the star. This suggests that this limit is strongly related to the GW torques [77,78] due to oscillations or asymmetries, although it could be due to the interaction of the accreting disk with the NS magnetic field [79]. The search for CWs from accreting sources is complicated mainly by two factors [76]: (i) the source is spun up by the companion during the accretion, and a spin-wandering effect [80] could be present; (ii) an additional Doppler effect by the binary orbital motion is present [81]. Eventually, variations in the matter accretion rate directly reflect into irregular spinning frequency. To make these searches even more complicated, often the spin frequency is not known, as in the case of Sco X-1.

Different approaches are used, tailored to the emission model considered for the search. For instance, some methods are adapted and/or new algorithms have been developed for the case of a long duration transient emitted by postmerger remnants, or for the case of CWs from glitching pulsars. In the postmerger remnant case, the source is expected to have a high spin-down rate; hence, the frequency will strongly vary with time. In the glitching pulsar case, the frequency suddenly changes, a sudden spin-up occurs, which may enhance the GW emission for a short time [82], and then the star relaxes back to the standard spin-down scenario.

In thee case of detection, it is possible to extract some information about the main CW emission mechanism happening in an NS, by looking at the GW frequency measured (see [13]). In particular, it is known that the GW frequency is related to the star spin frequency according to $f_{gw} = k(f_{spin} + f_{prec})$. Here, k is a proportionality factor dependent on the model considered. In the simplest case of no precessing ($f_{prec} = 0$) rigid rotating bodies, with asymmetries supported by elastic and/or magnetic stresses, $k = 2$, and hence, $f_{gw} = 2f_{spin}$. In r-mode oscillations scenarios, the estimated emitted frequency is $f_{gw} \sim \frac{4}{3} f_{spin}$, although deviations from this number are expected when relativistic corrections are included and/or different EOS are considered. In this case, the GW amplitude of the r-mode signal is parametrized in terms of the r-mode amplitude α, and it explicitly depends on the mass and radius of the NS and on the star EOS. For the case of CWs emitted by LMXB systems, accreting matter from a companion star, the relation between the spin frequency and the GW frequency is expected to be $f_{gw} = 2f_{spin}$.

As the star spins, its angular momentum will be radiated away, e.g., via GW emission, decreasing its frequency as [1]

$$\dot{f} = Kf^n \tag{8}$$

where the negative constant K and the braking index n depend on the energy loss mechanism as $n = f\ddot{f}/\dot{f}^2$. The spin-down process may be more complicated than the simple power law in Equation (8), and in general, it is possible that the energy loss is due to a simultaneous contribution from both the gravitational and magnetic dipole emission. For a spin-down fully dominated by a gravitational emission [83], i.e., a gravitar, $n = 5$ (or $n = 7$ if the GW emission happens via r-mode), while $n = 3$ for magnetic dipole emission. An estimate of the age of the source can be expressed as

$$\tau = -\left[\frac{f}{(n-1)\dot{f}}\right]\left[1 - \left(\frac{f}{f_0}\right)^{(n-1)}\right] \tag{9}$$

here, f_0 is the star birth rotation frequency. For old sources (with $f \ll f_0$), the age is simplified as

$$\tau \approx -\left[\frac{f}{(n-1)\dot{f}}\right] \tag{10}$$

More complicated emission scenarios are described in the literature. For instance, when the star is in free precession, dual harmonic emissions can be present at once and twice the star's spinning frequency. A particular case of dual harmonic emission is encountered when the star has a superfluid core pinned to the crust and not aligned with the principal

axes of the moment of inertia [84]. More complex emission models exist, e.g., when the configuration is that of a triaxial freely precessing body or for the case of a deferentially rotating two-component star. In this case, the emission may happen on more than two harmonics, complicating the signal waveform to be searched for. Typically these models are not considered in real searches.

The class of CWs signals is then a good benchmark to study the state of matter at higher densities. In addition to this aspect, CW detections can be used to test general relativity (GR). According to GR, only two tensor polarization states exist for GWs. When more generic metric theories of gravity are assumed, the number of polarizations increases up to six, allowing for two scalar and two additional vector modes. In particular, for the Brans–Dicke theory of gravity [85], only one additional scalar polarization state is predicted to be present along with the two tensor polarizations predicted by GR. As discussed in [86–88], it is possible to put constraints on these extra polarizations using CWs detections from known pulsars. Indeed, the detector response function to a given polarization depends on the direction of propagation of the GW along the two detector arms (see, e.g., [89]). Given the long duration nature of CWs, different antenna patterns will produce a different sidereal amplitude modulation. This means that all the relevant information to distinguish between the polarizations is encoded in the sidereal-day-period amplitude modulation of the signal. This is true only if the signal phase evolution for non-GR polarizations is equal to that assumed for GR.

Strain Amplitude Limits

It is possible to identify promising targets for CWs by computing some limits based on the information about the source. These quantities constraint the maximum GW emission of a given source. Three main limits are used in CW searches: the spin-down limit, the age-based limit and the torque balance limit.

Spin-down limit: generally, for known pulsars with precisely measured f_{spin} and $\dot{f}_{\text{spin}}$, it is possible to define the so-called spin-down limit on the maximum detectable strain [57]. If all the energy loss during the spin-down is released in the form of GWs, by equating the GW power emission to the time derivative of the rotational kinetic energy, one obtains a source at a distance r:

$$h_0^{\text{sd}} = \frac{1}{r}\sqrt{\frac{5}{2}\frac{G}{c^3}I_3\frac{|\dot{f}_{\text{gw}}|}{f_{\text{gw}}}} = 2.5 \times 10^{-25}\left(\frac{1\text{ kpc}}{r}\right)\sqrt{\left(\frac{1\text{ kHz}}{f_{\text{gw}}}\right)\left(\frac{|\dot{f}_{\text{gw}}|}{10^{-10}\text{ Hz/s}}\right)\left(\frac{I_3}{I_0}\right)}. \quad (11)$$

where $I_0 = 10^{38}$ kg m^2. This gives an absolute upper limit to the amplitude of the CW signal emitted by a pulsar.

Age-based limit: an alternative way to check the goodness of a potential CW target, when the rotational parameters are unknown, is to look at the so-called indirect age-based limit. Similar to the spin-down limit, assuming that all the energy lost is radiated away with GWs, it is possible to express the spin-down limits in terms of the age of the star τ using Equation (9) and a braking index $n = 5$ [90]

$$h_0^{\text{age}} = 2.27 \times 10^{-24}\left(\frac{1\text{ kpc}}{r}\right)\left(\frac{1\text{ kyr}}{\tau}\right)^{1/2}\left(\frac{I_3}{I_0}\right)^{1/2}. \quad (12)$$

Torque balance limit: empirical upper limits can also be defined for accreting binaries. Assuming that the GW emission is completely balanced by the angular momentum added via accretion, the so-called torque-balance limit can be derived [91]. Assuming that the accretion luminosity is fully radiated as X-rays, this provides an estimate on the mass accumulation rate; hence, the limit can be written in terms of the observable X-ray flux F_X and the star spin frequency (GW frequency):

$$h_0^{\text{tb}} = 5 \times 10^{-27} \left(\frac{F_X}{F_\star} \right)^{1/2} \left(\frac{R}{10 \text{ km}} \right)^{1/2} \left(\frac{r_m}{10 \text{ km}} \right)^{1/4} \left(\frac{1.4 \text{M}_\odot}{M} \right)^{1/4} \left(\frac{700 \text{ Hz}}{f_{\text{gw}}} \right)^{1/2} \tag{13}$$

with $F_\star = 10^{-8} \text{ erg cm}^{-2} \text{ s}^{-1}$. M and R are the NS mass and radius and r_m is the lever arm, usually equal to R or to the Alfven radius, i.e., the radius corresponding to the inner edge of the accretion disk.

2.2. Dark Matter Candidates

A CW-like signature is expected to be produced in the data also by several potential DM candidates [92]. For a few years, interferometric detector data have been used to look for evidence of DM, both in terms of GW, emitted by systems made up of particles from the dark sector, and as direct DM detectors, assuming a DM coupling to the detector components. For a review of all the DM candidates that can be investigated using GWs detectors, see [93]. Potential DM candidates may be ultra-light bosons, including dark photons or quantum-chromo-dynamic axions [94–97]. In this section, I review three main scenarios involving DM candidates, where a persistent CW-like signal is expected to be produced and actively searched by the CW community: boson clouds around spinning BHs, vector bosons in form of dark photons, compact dark objects or primordial black holes. The latest observational results will be discussed in Section 4.2.

2.2.1. Boson Clouds

Ultralight bosons condensates can clump around spinning BHs through superradiance [95,96,98]. The BH-boson cloud system can be described using an analogy with the hydrogen atom model when the axion's Compton wavelength is comparable to the size of a BH, turning this system into a "gravitational atom". When boson fields are present nearby a spinning BH, these can interact with the BH and condensate around it, all occupying the same (quantum) state and reaching huge occupation numbers after exponential growth. This process takes place at the expense of the BH angular momentum, and indeed, the axion or axion-like particles scatter on the BH decreasing its spin. When the BH spin is low enough, the superradiance process stops, and the cloud dissipates via axion annihilation into gravitons. During this depletion phase or when transitioning between levels of the gravitational atom, the system generates a quasi-monochromatic and long-duration signal that can be searched with CW methods. It should be noted, however, that the GW contribution from transition levels is sub-dominant. The most interesting scenario for Earth-based detectors such as LIGO, Virgo and KAGRA is the annihilation process. Indeed, the signal produced in this case is in the detector sensitivity band for boson masses in the $10^{-13} - \times 10^{-12}$ eV range. If the boson self-interaction is negligible, the gravitational-wave signal frequency depends mainly on the mass of the boson and weakly on the mass and spin of the BH. When self-interaction is considered, the approximation of the signal with a CW-like shape is no longer valid since the signal is strongly suppressed [99]. In particular, if the self-interaction is stronger than the gravitational binding energy, the cloud becomes unstable, and it collapses in a process known as "bosenova". During this process, the system may produce a burst of GWs [95]. In general, the annihilation signal cannot be fully characterized unless some assumptions on the BH are made. Indeed, the emitted signal depends on the mass, spin, distance, and age of the BH.

Let us briefly review the main characteristic of the signal emitted by BH-boson clouds as in [94,95,98,100,101]. When the superradiant condition is satisfied, i.e., when the boson angular frequency is less than the BH's outer horizon angular frequency, the scalar field starts to clump around the BH. This effect is maximized when the particle's reduced Compton wavelength $\lambda_b = \frac{\hbar c}{m_b}$, which depends on the boson mass m_b, is comparable to the BH Schwarzschild radius $R = \frac{2GM_{\text{BH}}}{c^2}$. This superradiant instability phase has a typical duration of

$$\tau_{\text{inst}} \approx 20 \left(\frac{M_{\text{BH}}}{10 \ M_\odot} \right) \left(\frac{\alpha}{0.1} \right)^{-9} \left(\frac{1}{\chi_i} \right) \text{ days}, \tag{14}$$

dependent on the BH mass $M_{\rm BH}$ and dimensionless spin χ_i. Returning to the analogy with the hydrogen atom, α is the fine-structure constant in the gravitational atom

$$\alpha = \frac{G M_{\rm BH}}{c^3} \frac{m_b}{\hbar}. \tag{15}$$

As long as the BH spin is above the critical spin $\chi_c \approx \frac{4\alpha}{1 + 4\alpha^2}$, the cloud will continue to grow and the BH will decrease its spin. Once equilibrium has been reached, the boson cloud mass is dissipated on a timescale[2]

$$\tau_{\rm gw} \approx 6.5 \times 10^4 \left(\frac{M_{\rm BH}}{10 \, M_\odot} \right) \left(\frac{\alpha}{0.1} \right)^{-15} \left(\frac{1}{\chi_i} \right) \text{ years.} \tag{16}$$

The GW amplitude decays in time as $\left(1 + t/\tau_{\rm gw} \right)^{-1}$ from a starting strain amplitude determined mainly by the BH and boson masses (entering in the definition of α) and the BH initial spin

$$h_0 \approx 3 \times 10^{-24} \left(\frac{\alpha}{0.1} \right)^7 \left(\frac{\chi_i - \chi_c}{0.5} \right) \left(\frac{M_{\rm BH}}{10 \, M_\odot} \right) \left(\frac{1 \, {\rm kpc}}{r} \right). \tag{17}$$

During this emission phase, the GW emitted frequency, which is twice the frequency of the field, is also dependent on the two-component masses as

$$f_{\rm gw} \simeq 483 \, {\rm Hz} \left(\frac{m_b}{10^{-12} \, {\rm eV}} \right) \left[1 - 7 \times 10^{-4} \left(\frac{M_{\rm BH}}{10 \, M_\odot} \frac{m_b}{10^{-12} \, {\rm eV}} \right)^2 \right] \tag{18}$$

During the depletion phase, a small spin-up is present due to the loss of mass. Indeed, during the cloud formation phase, a large spin-down rate is present, although the expected signal strain is still too low to be detected. This drift changes when the cloud starts to evaporate. The actual spin-up rate during the depletion phase is strongly dependent on the boson self-interaction constant. For simplicity, we consider the case of a negligible self-interaction when the spin-up due to annihilation is the dominant drift:

$$\dot{f}_{\rm gw} \approx 7 \times 10^{-15} \left(\frac{m_b}{10^{-12} \, {\rm eV}} \right)^2 \left(\frac{\alpha}{0.1} \right)^{17} \text{ Hz/s.} \tag{19}$$

When the self-interaction starts to be non-negligible, the spin-up rate is enhanced by two contributions, one from the bosons energy level transition and a second from the change in the self-interaction energy as the cloud depletes. At this point, the signal is expected to be shorter or with a smaller amplitude. For a more general discussion on the role of the boson self-interaction parameter, see [99]. In current CW searches, the main contribution to the GW emission considered for these models are those from the main growing state since the second fastest growing state emission is weaker than the first level one and is not fully quadrupolar.

Analogous to the standard CW case for NSs, Doppler modulations should be considered when looking for the signal in the detector data (see Section 4.2 for the latest observing results from this field). Finally, we notice that the same superradiance effect described above is somehow expected also for rotating NS [102,103], although it is not clear if the GW emission is loud enough to be detected by currently operating detectors.

2.2.2. Ultralight Vector Bosons: Dark Photons

DM particles are expected to interact with other DM particles in the same way as standard matter interacts with the EM force mediated by the photon. The equivalent force mediator for the dark sector is the dark photon. According to current theories, the dark photon is not expected to couple directly to standard model particles, although a small mixing-induced coupling to EM currents can be present [104,105]. Here, we focus

on an ultralight DM candidate, which behaves as a classical field interacting coherently with the atoms of the test masses. In particular, we assume that the dark photon is a vector boson coupled to the baryon or baryons minus leptons number $U(1)_B / U(1)_{B-L}$. In practice, if sufficiently light, the dark photon has a high phase-space density; hence, it behaves as a coherently oscillating classic field producing an oscillating force on dark charged objects [106–108]. The same type of oscillation is expected for the tensor boson case [109]. The mass of the dark photon could be provided either by a dark Higgs boson or via the Stuckelberg mechanism [104,105,110]. Different production mechanisms have been proposed for the dark photon, such as the misalignment mechanism associated with the inflationary epoch, light scalar decay or cosmic strings [111,112]. Several attempts to set constraints on this type of DM are present in the literature [107,113,114]. The dark photon DM field oscillations act as a time-dependent equivalence principle-violating force acting on the test masses and producing a change in the relative length of the detector's arms. There exist two main signatures when test bodies interact with the dark photon fields: a spatial gradient is present, producing a relative acceleration between the objects due to the different field amplitude; given the equivalence principle-violation of this force, test masses of different materials will experience different accelerations. For all Earth-based detectors, an additional effect due to the finite light travel time should be considered [115,116].

I briefly review the main characteristics of the expected signal from dark photons while search results are discussed in Section 4.2. The Lagrangian of the massive vector field A^μ, which couples to B or $B-L$ current $J_D^\mu (D = B$ or $B-L$) as DM is given (in natural units) by

$$\mathcal{L} = -\frac{1}{4} F^{\mu\nu} F_{\mu\nu} + \frac{1}{2} m_A^2 A^\mu A_\mu - \epsilon_D e J_D^\mu A_\mu, \tag{20}$$

where $F_{\mu\nu} = \partial_\mu A_\nu - \partial_\nu A_\mu$, m_A is the mass of the vector field, and ϵ_D is the coupling constant normalized to the EM one. The dark photon field A_μ can be approximated as a plane wave with a characteristic momentum $\vec{k} \simeq m_A \vec{v}_0 / \hbar$, within a coherence time $T_{\mathrm{coh}} \simeq 2\pi\hbar (m_A v_0^2)^{-1}$. The local amplitude $A_{\mu,0}$ of the dark electric gauge field is obtained assuming an energy density, $\frac{1}{2} m_A^2 A_{\mu,0} A_0^\mu$, equal to that of the local DM $\rho_{\mathrm{DM}} = 0.4 \, \mathrm{GeV/cm^3}$. The time-dependent force acting on the test masses produces a strain oscillating at the same frequency and phase as the DM field [106,116–118]. It should be noted that a similar signal may be produced in the case of scalar dark matter particles directly interacting with the mirrors. In particular, as described by [119], the interaction of the scalar bosons with the beam-splitter will induce oscillations in the thickness of the mirror due to the oscillations of the fundamental constants [120–122]. Considering only vector bosons in a non relativistic scenario, the contribution from the magnetic dark field is negligible if compared to the electric dark field[3]. The dark photon DM background field will generate an acceleration on each i-th test mass as:

$$\vec{a}_i(t, \vec{x}_i) = \frac{\vec{F}_i\left(t, \vec{x}_i\right)}{M_i} \simeq \epsilon_D e \frac{q_{D,i}}{M_i} \partial_t \vec{A}\left(t, \vec{x}_i\right) \tag{21}$$

M_i and $q_{D,i}$ are the total mass and dark charge of the test mass located at x_i.

This acceleration will cause a tiny differential relative displacement between pairs of test masses that can be converted into a strain by integrating Equation (21) twice over time. Following [116,123], the GW strain will have two contributes, one due to the relative variation of the arm length due to the dark force acting on the mirrors $h_D(t)$, and a second one due to the finite light-traveling time in the arm $h_C(t)$. These two contributions can be averaged over random polarization and propagation directions, and the resulting strain in SI units can be written as:

$$\sqrt{\langle h_D^2 \rangle} = C \frac{q}{M} \frac{e \epsilon_D}{2\pi c^2} \sqrt{\frac{2 \rho_{\mathrm{DM}}}{\epsilon_0}} \frac{v_0}{f_0} = 6.28 \times 10^{-27} \left(\frac{\epsilon_D}{10^{-23}} \right) \left(\frac{100 \, \mathrm{Hz}}{f_0} \right) \tag{22}$$

$$\sqrt{\langle h_C^2 \rangle} = \frac{\sqrt{3}}{2} \sqrt{\langle h_D^2 \rangle} \left(\frac{2\pi f_0 L}{v_0} \right) \simeq 6.21 \times 10^{-26} \left(\frac{\epsilon_D}{10^{-23}} \right). \tag{23}$$

The total strain will be the root sum of the squares of the two contributions. The quantity C is a geometric factor dependent on the position and orientation of the interferometer with respect to the DM wind. The signal frequency is then determined by the dark photon mass $f_0 = m_A c^2 / (2\pi\hbar)$, corresponding for Earth-based detectors to dark photon masses in the range 10^{-14}–10^{-11} eV/c^2. Given that the velocity of dark photon particles follows a Maxwell–Boltzmann distribution, and assuming a virial velocity of $v_0 = 220$ km/s, the signal frequency will lie in the $(f_0, f_0 + \Delta f)$ range, where:

$$\frac{\Delta f}{f_0} = \frac{1}{2} \frac{v_0^2}{c^2} \approx 2.94 \times 10^{-7}. \tag{24}$$

Furthermore, for the dark photon DM case, the Doppler shift due to Earth's rotation is present, although the frequency shift due to this effect is an order of magnitude smaller than the one from the Maxwell–Boltzmann spreading.

2.2.3. Compact Dark Objects and Primordial Black Holes

Dark matter can be present in our Universe in the form of macroscopic objects, which we generically refer to as compact dark objects (CDOs). The actual formation channel and the origin of CDOs are still widely debated. According to some hypotheses, CDOs can be also PBHs. CDOs can form pairs and emit an almost monochromatic signal while being far from the coalescence phase. One option for the formation of the pair, proposed in [124], is to assume that these objects can be trapped inside normal matter via non-gravitational interactions, for instance, the Sun or even the Earth [125]. If a second CDO is also trapped inside the same object, these can form a binary CDO emitting GWs with a long lifetime for low mass objects. According to [124], the probability of collisions between CDOs and the Sun is not negligible for CDOs masses $\sim 10^{-10} M_\odot$; hence, there is a non-negligible possibility of having these pairs of CDOs formed in our solar system. Furthermore, PBHs can be constituents of a fraction of the DM in the Universe depending on their formation channels (see [126–129] for the latest reviews about PBHs as DM candidates). In particular, the origin of most of the sub-solar and planetary mass BHs is likely primordial, although speculations on alternative formation channels exist, e.g., created from NSs by the accumulation of DM and subsequent collapse into a BH [130]. For the context of CW signals, PBHs, as well as more generic CDOs, represent potential targets. Indeed, the GW signals emitted by these systems, when the two compact objects are far away from the coalescence and/or their masses are small enough, are modeled as quasi-monochromatic. This approximation is valid until the inspiral orbit does not reach the inner-most stable orbit. When the low-mass/far-from-coalescence conditions are dropped, the frequency evolution of these systems is better represented by a power law with a spin-up.

For the masses considered ($\leq 10^{-5} M_\odot$) in searches for CW signals from a pair of compact objects, the linear approximation is always valid considering the frequencies of the detector sensitivity band. In addition, if the chirp mass is small enough, the frequency can be modeled exactly as the linear frequency Taylor expansion used for standard CW searches. This means that, for instance, a pair of inspiralling PBHs with chirp masses below 10^{-5} $M_\odot$ would emit a GW signal indistinguishable from those arising from non-axisymmetric rotating NSs spinning up.

Let us now consider the type of emission that could be released by these systems. The two systems of the two orbiting PBHs/CDOs can be approximated as a two-body problem of point mass objects in a circular orbit. The system loses energy as the inspiralling continues and the two masses approach each other. The signal model discussed in this section is widely described in the classical handbook of GW science [131–133] as well as

in [124,134–136]. The expected signal strain amplitude is that of a circular BH binary inspiral at a distance r identified by a chirp mass $\mathcal{M}$ with a time to the coalescence $\tau = t_c - t$:

$$h_0(t) = \frac{4c}{r} \left(\frac{G\mathcal{M}}{c^3} \right)^{5/3} \left(\pi f_{\text{gw}}(t) \right)^{2/3}. \tag{25}$$

The amplitude is time-dependent and scales with the GW frequency, equal to twice the system orbital frequency. The GW frequency emitted is dependent on the system chirp mass $\mathcal{M}$ as

$$f_{\text{gw}}(\tau) = \frac{(5/\tau)^{\frac{3}{8}}}{8\pi} \left(\frac{G\mathcal{M}}{c^3} \right)^{-5/8}. \tag{26}$$

In this case, the expected signal frequency variation (the spin-up) due to the change in distance of the inspiralling system is given by:

$$\dot{f}_{\text{gw}} = \frac{96}{5} \pi^{8/3} \left(\frac{G\mathcal{M}}{c^3} \right)^{5/3} f_{\text{gw}}^{11/3}. \tag{27}$$

Equation (26) is derived by integrating the expression for the spin-up. For low masses, the frequency evolution can be simplified, assuming that the observing time T_{obs} is bigger than τ and assuming a small chirp mass. This means that the PBH/CDO spin-up rate $\dot{f}_{\text{gw}}$ can be treated as a constant. In this case, the expected signal can be linearized as $f_{\text{gw}}(t) \sim f_0 + (t - t_0)\dot{f}_{\text{gw}}$, which coincides with the standard NS case (see Equation (29)). On the other hand, if the spin-up is too high, this approximation is no longer valid, and the frequency evolution should be modeled as a power-law, as discussed in [136]. Furthermore, for this system, the signal undergoes a daily modulation at the detector, which should be considered in the analyses.

3. Searches for CWs Signals with Earth-Based Detectors

Different methods for the search for CW signals have been developed. The variety of methods reflects the different ways it is possible to look for these long-lasting signals, giving priority to the sensitivity of the pipeline (i.e., the search algorithm) or its robustness with respect to deviations of the signal from the assumed model.

3.1. The Signal at the Detector

CWs are by definition all those quasi-monochromatic GW signals characterized by a long duration, ranging from hours to years, and deeply buried in detector noise. When the CW signal reaches the detector, several modulation effects occur. The strain measured at the detector for a triaxial rotor is given by

$$h(t) = h_0 \left[F_+(t, \alpha, \delta, \psi) \frac{(1 + \cos^2 \iota)}{2} \cos \Phi(t) + F_\times(t, \alpha, \delta, \psi) \cos \iota \sin \Phi(t) \right] \tag{28}$$

here, (α, δ) are the right ascension and declination of the source in the sky, ψ is the polarization angle, $F_{+/\times}$ are the detector response to the two $h_{+/\times}$ polarizations of the GW. The signal strain also depends on the inclination of the rotation axis to the line of sight ι and the GW phase $\Phi(t)$ (see, e.g., [132]). The phase of the GW signal is related to the frequency components $(f, \dot{f}, \ddot{f}, \ldots)$ at a given reference time t_0 as

$$\Phi(t) = \phi_o + 2\pi \left[f(t - t_0) + \frac{\dot{f}}{2!}(t - t_0)^2 + \ldots \right] \tag{29}$$

where ϕ_0 is an initial phase. The signal phase is modulated mainly by the Doppler due to relative motion between the detectors and the source and other relativistic effects, namely the Einstein and Shapiro delays. The frequency at the detector will be spread with respect to the emitted frequency as:

$$f_{\text{gw}}(t) = \frac{1}{2\pi}\frac{d\Phi(t)}{dt} = f_0(t)\left(1 + \frac{\vec{v}(t)\cdot\widehat{n}}{c}\right) \tag{30}$$

where $\vec{v}$ is the velocity vector of the detector, while $\widehat{n}$ is the unit vector pointing to the source direction, both expressed in the Solar System Barycenter reference frame. Here, $f_0(t)$ is the GW frequency arriving at the detector at the time t and emitted by the star at the reference time t_0. As mentioned in the previous sections, $f_0(t)$ can be described by a Taylor expansion such as $f_0(t) \simeq f_0 + \dot{f}(t - t_0) + \ldots$, where $\dot{f}$ is the first order spin-down parameter.

The phase modulation due to the Doppler Effect, apart from an irrelevant constant, can be obtained by integrating Equation (30) as:

$$\phi_d(t) = 2\pi \int_{t_0}^{t} f_0(t') \frac{\vec{v}\cdot\widehat{n}}{c} dt' \approx \frac{2\pi}{c} p_{\widehat{n}}(t) f_0(t) \tag{31}$$

where $p_{\widehat{n}}(t)$ is the position of the detector projected along $\widehat{n}$.

The pure signal strain at the detector, assuming the ideal situation where no noise is present, is depicted in Figure 1.
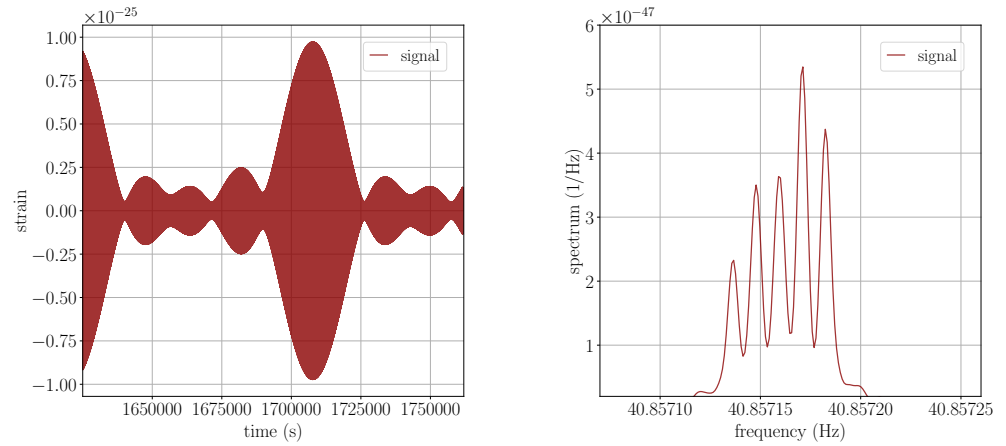
Figure 1. Features of a CW signal without noise. (**Left**): time series of the signal before removing any modulation, the signal is modulated in amplitude and frequency. (**Right**): power spectrum after removing the frequency modulations, the five peaks due to the sidereal modulation are clearly visible.

The figure on the left reproduces a signal as it is received at the detector, and it is visibly modulated both in frequency and in amplitude. Even after the removal of the main modulation effects, namely the Doppler and the spin-down of the source, the power spectrum reported on the right side is very different from the one produced by a purely sinusoidal signal. This amplitude modulation is produced by the antenna sidereal response; hence, by the time dependence of $F_{+/\times}$. In the right plot, five peaks are visible, and those are due to the Earth's sidereal modulation. This last effect produces a splitting of the signal power among five frequencies f_0, $f_0 \pm f_\oplus$ and $f_0 \pm 2f_\oplus$, where $f_\oplus$ is the Earth's sidereal frequency. In a more general formalism where a dual-harmonic emission is assumed, the strain at the detector has two components h_{21} and h_{22}, representing the emission at f_{spin} and $2f_{\text{spin}}$, respectively (see, e.g., Equations (1) and (2) in [137]). The two harmonics are typically represented by the two amplitudes C_{21} and C_{22}. Equation (28) is equivalent to the h_{22} component only, i.e., which corresponds to the case of $C_{21} = 0$ and $C_{22} = h_0/2$.

When the signal is buried in the detector data, it is not possible to appreciate the signal morphology by eye since it is several orders of magnitude lower than the typical data strain amplitude. For this reason, effective data analysis methods are needed to extract the signal from the noise. Some of these methods are reported in the following section, while the results will be discussed in Section 4.

3.2. Search Methods

Given the long-lived and weak nature of CW signals, it is intuitive to think that the more data that are used in the analysis, the more signal power is accumulated, thus increasing the signal-to-noise ratio. The optimal search method to look for these signals, provided that the waveform is completely known and under the assumption of gaussian noise, is the matched filtering. Several methods have been developed to look for sources such as know pulsars, where all the parameters of the source are known. Source parameters may be available from EM observations, i.e., the source sky position and its rotational parameters are known. In this case, the so-called "targeted" searches are performed using matched filtering. Several implementations of the matched filtering techniques, also known as coherent searches, exist based on different detection statistics or algorithms: the `5-vector` [138,139] method, the `F/B/G statistic` [140–144] and the time-domain heterodyne-based pipelines (`Bayesian` and `Band-Sampled-Data`) [145–147].

In targeted searches, the phase of the CWs is assumed to be locked to the rotational phase of the crust of the star, which is completely defined by its EM observation. When this assumption is relaxed, "narrow-band" searches are performed. This would allow taking into account, e.g., a differential rotation between the rigid crust and superfluid parts of the star. In these searches, a small region around the EM-inferred signal parameters is investigated. In general, a narrow-band search for a given target is less sensitive than its respective targeted case due to the increased trial factor.

As the knowledge about the source parameters decreases, the parameter space to investigate explodes, making the use of fully coherent searches impractical [148]. For this reason, many semi-coherent techniques have been developed [149,150]. In a typical semi-coherent search, chunks of data may be first analyzed coherently (e.g., using a matched-filter) and then combined incoherently (i.e., not considering the phase information). This incoherent combination can be achieved in many different ways, for instance, by summing the detection statistics in each chunk of data analyzed and computing a single final detection statistic (see [12] for a detailed review of wide parameter space searches for CWs). These searches are suitable in the case when no EM counterpart is present, such as all-sky search surveys for NS or DM candidates, or when the true nature of the source is not completely known, for instance, directed searches pointing to interesting sky regions or supernova remnants hosting potential young NS. Semi-coherent methods include the `FrequencyHough` [151–153], the `SkyHough` [154–156], the `Time-Domain` $\mathcal{F}$`-statistic` [140,157,158], `Weave` [159], `PowerFlux` [160,161], and `Einstein@Home`, based on the global correlation transform method [162–164]. A comparison of methods for the detection of GWs from unknown NSs is given in [165].

Loosely coherent methods, such as the `Falcon` pipeline [166–168], have been developed to manage the huge computing cost of all-sky searches while keeping the robustness to a wide family of signals, allowing for a loose phase track in the evolution of the signal frequency. A different approach can be used if one wants to go deep with the sensitivity in an all-sky search but keep the focus on a specific narrow frequency band, as described in [169].

Semi-coherent or incoherent methods can be used when no assumption on the source frequency evolution is made or if it is different from the standard Taylor expansion in time such as in Equation (29). These include the hidden Markov model `Viterbi` tracker [170–172], the `Sidereal Filter` [173] and cross-correlation based methods such as `CrossCorr` [174] `STAMP` [175], `SOAP` [176] or `Radiometer` [177]. Some of these methods—CrossCorr method [178], Viterbi/J-statistic method [179], the 5-vector binary method [180] and the method in [81]—have been adapted for the LMXB searches such as Sco-X1, where also the orbital modulation needs to be considered and a stochastic spin wandering, including spin-up, is sometimes taken into account. Methods specifically tailored for all-sky searches for unknown binaries are the `BinarySkyHough` [181] and `TwoSpect` [182].

Different flavors of the above-mentioned techniques have been adapted for the case of long-transient CW signals [183–189] and glitching pulsars [190,191], ensemble of pul-

sars [144,192,193] or DM candidates [194–196]. Furthermore, several methods have been developed for the search of CW signals using machine learning [197–203]. For the latest review on CW methods and searches, see [12,14,16].

In general, all these pipelines produce the so-called search candidates, i.e., potential astrophysical signals that need to be investigated in detail. These candidates undergo a series of post-processing veto steps, and then, the most interesting ones are followed up with different techniques in order to clearly establish their significance, e.g., [203–214]. A fraction of these candidates is vetoed if found near known instrumental artifacts, also known as spectral lines, typically present in the detectors [215]. Multiple approaches exist for this part of the analysis to discard or pass the outliers to the follow-up stage, as described in [12]. Sometimes the assessment of the real origin of an outlier is the most difficult and less automatized part of the analysis, but in general, for most of the follow-up techniques, the final goal is to check if the outlier significance follows an expected theoretical trend. This is achieved, for instance, by checking if the outlier signal-to-noise ratio grows as more data are used to analyze that candidate or by increasing the coherence time. Alternative follow-up methods are based on machine learning techniques (see Section 4 in [12]).

If all the outliers are discarded from being real astrophysical signals during the follow-up stage, no CW signal detection can be claimed. In this case, typically upper limits on the signal strain are provided. These values usually span the full frequency range investigated in the search for the case of wide parameter space searches. For a given confidence level, the upper limit curve determines a watershed on the signal amplitude h_0 above which it is possible to exclude the existence of CW signals. These curves are estimated using a tremendous number of simulated signals added to the data or via less computationally expensive methods based on analytically derived or scaling formulas (the most famous being the "sensitivity depth" [212,216], see also [217,218]). In addition to giving an estimate of how deep a given search can look for a CW signal, upper limits are often used to set astrophysical constraints on some related quantities according to the type of search performed. Typical constraints derived from upper limit curves are those on the ellipticity of the spinning NS (or the quadrupole Q_{22}) or the r-mode amplitude α. In searches looking for DM candidates, these limits can be converted to, e.g., a coupling constant, mass exclusion regions, merging rates and abundances.

According to population studies, an order of 10^8–10^9 NSs is expected to exist in our Galaxy [219]. Only a small fraction of the expected population has been detected electromagnetically or has an associated EM counterpart [220]. Among all the $\sim$3000 sources reported in the Australian Telescope National Facility (ATNF) catalog [221], about 10% are in a binary system. If sources spinning at frequencies above 10 Hz are considered, this fraction increases to $\sim$50%. Information provided by astronomers is used to constrain the investigated parameter space. In this sense, CW searches have a strong multi-messenger approach. EM information is fundamental for the search of known pulsars, but it provides interesting inputs for the search of new sources, such as supernova remnants potentially hosting an NS, as well as updated information about these sources. In particular, the detection of CWs from a particularly interesting source or sky region (galactic center, globular clusters, etc...) represents a real discovery; given the long-lasting nature of the signal, EM observations following the detection could be carried out for a long time, opening the possibility to, e.g., perform tests of GR and/or to set interesting constraints on the inner composition of the emitting body and on its EOS. On the other hand, the discovery of EM dark sources, including DM candidates, will provide a new tool for the study of a new population of astrophysical sources, as well as contribute to solving many of the open questions about our Universe.

4. Recent Results

Since the beginning of the advanced detector era, the interest with respect to CW sources has increased, as probed by the increasing number of publications on this topic over the years. Boosted by the enhancement of the sensitivity of the detectors as well as

the development of data analysis techniques, different and new searches have taken place. I briefly review the most recent search results for CW signatures in advanced detector data from the latest three observing runs [4,5,7]. The first observing run (O1) started on 11 September 2015 and finished on 19 January 2016. The second observing run (O2) lasted from 30 November 2016 to 25 August 2017. During O1, only the two LIGO interferometers were recording data, while during O2, the Advanced Virgo joined the run at the beginning of August 2017. The O3 run started on 1 April 2019, 15:00 UTC and finished on 27 March 2020, 17:00 UTC. In the following, we refer to the period 1 April 2019–1 October 2019 as O3a, while the second part of O3, O3b, starts on 1 November 2019 after a month-long commissioning break. Wherever possible, the latest and most stringent results will be presented at the beginning of each section, while older results will follow.

4.1. Results from Known Sources (Pulsars, LMXBs, Supernova Remnants)

In this section, I review the latest results for searches of CW from known sources or sources with an EM counterpart, such as the central compact objects in supernova remnants.

4.1.1. Known Pulsars

A targeted search is the most sensitive way to look for persistent signals from known pulsars. These searches strongly rely on the EM information available about the source. Indeed, in these searches, the GW phase evolution is completely determined by the EM observations of the rotational parameters of the star. This in principle gives a full picture of the GW emission from the star. A slightly different type of search, known as narrow-band, is sometimes applied if the coupling model between the GW and EM signal phase evolution is relaxed. This allows to assume a more generic scenario, and typically, a small region around the expected GW frequency and spin-down is investigated.

The latest extensive search for CW from known pulsars is reported in [222]. In this work, 236 pulsars have been analyzed, among which the Crab and the Vela pulsars, using LIGO and Virgo O3 data combined with O2 data. Several pulsars glitched during the considered runs and some have sufficient information from EM observations on their orientation to restrict their priors on the ι and ψ parameters. The ephemerides come from the observations from the CHIME, Hobart, Jodrell Bank, MeerKAT, Nancay, NICER and UTMOST observatories. The search was run using three independent pipelines: the time-domain Bayesian method [145,146], the F/G/D-statistic method [88,140,143] and the 5-vector method [138,139]. All the pipelines searched for the standard single harmonic GW emission from the $l = m = 2$ mass quadrupole mode with a frequency at twice the pulsar rotation frequency. In addition, the Bayesian and the F/G/D-statistic pipelines assumed a dual harmonic emission scenario, i.e., the $l = 2; m = 1, 2$ modes with a GW frequency at once and twice the rotation frequency [84,223]. To complete the search, the 5-vector method limited the search to the single harmonic scenario but at the $l = 2; m = 1$ mode only, hence assuming a GW frequency at the star rotation frequency. Furthermore, the D-statistic has been used to test the dipole radiation as predicted by the Brans–Dicke theory [85,88]. No GW detection has been reported, and upper limits on the strain are given in Figure 2. Blue stars indicate the upper limit of a given pulsar, and those with upper limits below the spin-down limit (see Equation (11)) are marked with yellow circles. Grey triangles mark the spin-down limit of each pulsar. The pink curve is a sensitivity estimate for a generic targeted search, and it is given by $\sim 10 \sqrt{S_n(f)/T_{\rm obs}}$, where $S_n(f)$ is the power spectral density.

From Figure 2, it can be seen that 23 out of the 236 pulsars have strain amplitudes lower than the limits calculated from their electromagnetically measured spin-down rates. Among these, 90 millisecond pulsars have a spin-down ratio, i.e., the ratio between the upper limit and the spin-down limit, less than 10. For instance, J0437-4715 and J0711-6830 have spin-down ratios of 0.87 and 0.57, respectively. For the Crab and Vela pulsars, these limits are factors of $\sim$100 and $\sim$20 lower than their spin-down limits, respectively. Nine of these twenty-three pulsars beat their spin-down limits for the first time. The pulsar with

the smallest upper limit on h_0 was J1745-0952 with 4.72×10^{-27}. The best Q_{22} upper limit was achieved by J0711-6830 with 4.07×10^{29} kg m^2, equivalent to a limit on the ellipticity of 5.26×10^{-9}. This result is lower than the maximum values predicted for a variety of NS equations of state [63]. Concerning the dual harmonic search, the most constraining upper limit for C_{21} was 7.05×10^{-27} for J2302+4442. The stringent C_{22} upper limit was 2.05×10^{-27} for J1537-5312.

A previous search using O1 plus O2 data on 222 pulsars is given in [224]. In that search, the percentage of GW emission contributing to the spin-down luminosity for Crab and Vela pulsars was less than 0.017% and 0.18%, respectively. Compared to the O2+O3 search [222] described above, these numbers decrease as expected to 0.009% for Crab but increased for Vela up to a maximum of 0.27%. This unexpected result is due to the presence of a significant noise line in the LIGO Hanford detector at twice Vela's rotational frequency during O3. The O1+O2 search in [224] and the O2+O3 search in [222] certainly improve the results of the previous "CW pulsar catalog" for 200 pulsars in O1 data [225].

Tests for non-GR polarizations are also provided for the 23 pulsars beating the spin-down limit in [222], checking for the additional non-negligible scalar radiation originated from the time-dependent dipole moment [88]. No deviation from GR has been reported, and the stringent upper limit for dipole radiation is obtained for the millisecond pulsar J0437-4715. A previous test on GR from known pulsar searches, not assuming any particular alternative theory of gravity, is given in [226] using O1 data.
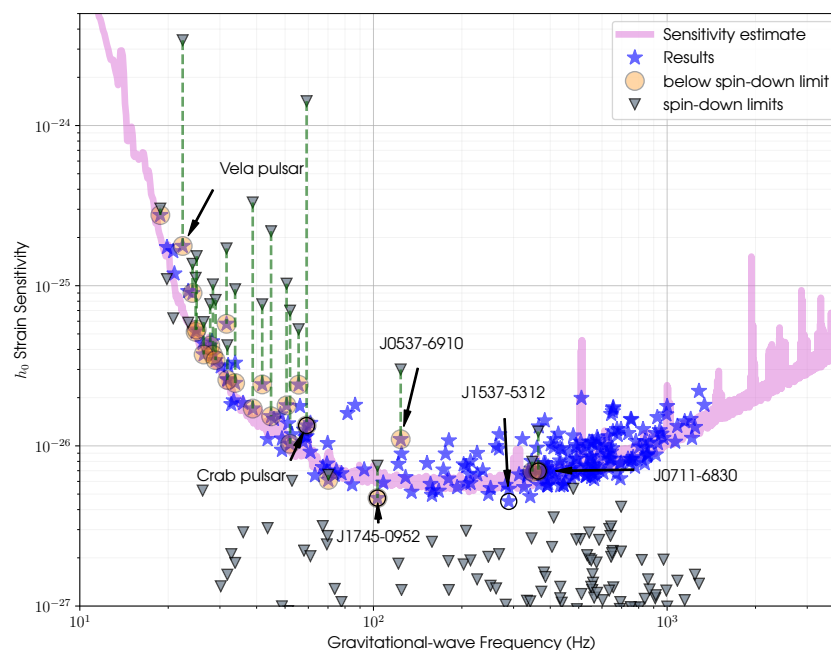
Figure 2. Upper limits on h_0 for the 236 pulsars in the targeted search in [222] are relative to the time-domain Bayesian method. The stars show 95% credible upper limits on the amplitudes of h_0. Grey triangles represent the spin-down limits for each pulsar computed as in Equation (11). Pulsars with upper limits surpassing their spin-down limits are marked with yellow circles. The pink curve gives an estimate of the expected strain sensitivity of all three detectors combined during the course of O3. Figure taken from [222].

A separate dual harmonic search has been performed on the same dataset (O2+O3) for the energetic young pulsar and frequent glitcher PSRJ0537-6910 in [227]. No CW signal has been detected in this search but, for the first time, the spin-down limit for this type of GW emission on this source has been surpassed. Results show that GWs from the $l = m = 2$ mode contribute to less than 14% of the spin-down energy budget. The same target has been investigated by two other searches, tuned for r-modes oscillations, using ephemerides from

NICER [228] in O3 [229] and O1+O2 [230] data. As discussed in Section 2.1, the relation between the gravitational-wave frequency and the star spin frequency in r-mode emission scenarios strongly depends on the NS structure. For this reason, both searches assumed the frequency evolution model proposed in [75]. Searches for the r-mode emission from PSRJ0537-6910 are motivated by the fact that this pulsar shows a trend in the inter-glitch behavior that suggests an effective braking index close to $n = 7$ at long times after the glitch [231,232]. A braking index of seven is expected for a spin-down dominated by the r-mode emission. The amplitude's upper limits in the O3 search [229] improve the existing results by a factor of up to three, placing stringent constraints on theoretical models for r-mode-driven spin-down in PSR J0537-6910. Another search for r-mode emissions for the Crab pulsar is reported in [233], providing for the first time upper limits beating the spin-down limit for this source/type of emission in O1 plus O2 data.

Five sources have been the target of a previous single and dual harmonic search for known pulsars [137]. These pulsars have been analyzed in the data from the first two and the first half of the third observing run of advanced detectors (O1+O2+O3a). The targets included three recycled pulsars[4] (J0437-715, J0711-6830, and J0737-3039A) and the two young pulsars Crab and Vela. For Crab, Vela and J0711-6830, a narrow-band search has also been performed using the 5-vector narrow-band method [234,235]. Results from this work constrain the equatorial ellipticities of some of the targets to be less than 10^{-8}, and for the first time, an upper limit below the spin-down limit for a recycled pulsar is reported. This latter aspect is interesting since the evolutionary history of a recycled pulsar is connected to an early accretion phase from a binary companion, very different from the case of young and more slowly spinning pulsars. Another set of seven recycled pulsars is investigated in [236]. The timing information is provided by the Arecibo 327 MHz Drift-Scan Pulsar Survey, and the search is performed on O1+O2+O3a data. All the targets, except for the millisecond pulsar J0154+1833, are in binary systems. The stringent constraint on the ellipticity is 1.5×10^{-8} for PSR J0154+1833.

Data from Fermi-LAT observations have been used in the search for CW from single harmonic emission from PSR J0952-0607 [237] and dual-harmonic emission from PSR J1653-0158 [238], using data from O1 and O2. The results of the search for CW signals from ten sources associated with TeV sources observed by the High Energy Stereoscopic System (H.E.S.S.) are reported in [239]. All the sources are associated with isolated NSs and with estimated distances up to 7 kpc. In particular, two targets are γ-ray pulsars, while eight H.E.S.S. sources are pulsar wind nebulae powered by known pulsars. The ephemerids for each pulsar are provided by the ATNF pulsar catalog. The search is performed using O2 data and tracks, with a hidden Markov model, the three GW frequencies expected to be at 1x, 2x and 4/3x the source spin frequency in a narrow band of 1 Hz around each multiple.

The latest results from the O3 fully coherent narrow-band search can be found in [240]. The search looks for CW from 18 pulsars using the five-vector and F-statistic narrow-band pipelines. For seven of these pulsars, the upper limits are lower than their spin-down limit. These results overcome the corresponding ones from the narrow-band search in O3a [137], improving the upper limits by a factor ~35% for the Crab pulsar, and ~10% for Vela and J0711-6830 pulsars even if the parameter space investigated in this search is 6.5, 1.2 and 7.1 times larger. Results from an additional search for long-duration transient GWs after pulsar glitches are also reported in [240]. Six targets have been investigated by the long-transient search, performed using the transient F-statistic method [185,241]. For these six sources, showing a total of nine glitches, an independent long-transient search is performed after each glitch. None of these targets, neither from the narrow-band or long-transient search, produced an outlier significant enough to be considered as a signal, although two marginal outliers are reported for the last glitch of J0537-6910. The transient F-statistic method has been applied for the search of long-duration transients after glitches in the Vela and Crab pulsars in O2 data [242]. Previous narrow-band searches using O2 and O1 data are given in [243,244].

4.1.2. Supernova Remnants

Another family of interesting targets with EM counterparts, but without precise timing of the rotational parameters, is the supernova remnants. Supernova remnants may host young NSs, which are excellent targets for the search for CWs. Given the lack of information on the spin frequency of the central compact object inside the nebula, directed searches are performed. In these searches, the only information assumed as known is the source sky position, while the remaining parameters $(f, \dot{f}, \ldots)$ are investigated in a wide range. The choice of the parameter space to investigate is only limited by the computing cost of the search, and this may change according to the different algorithms used and to the specific setup chosen. Given an amount of computing power, some regions may have a higher priority over the full GW sensitivity band [245,246]. No CW detection is reported from these sources. In the following, I report the latest search results from these targets.
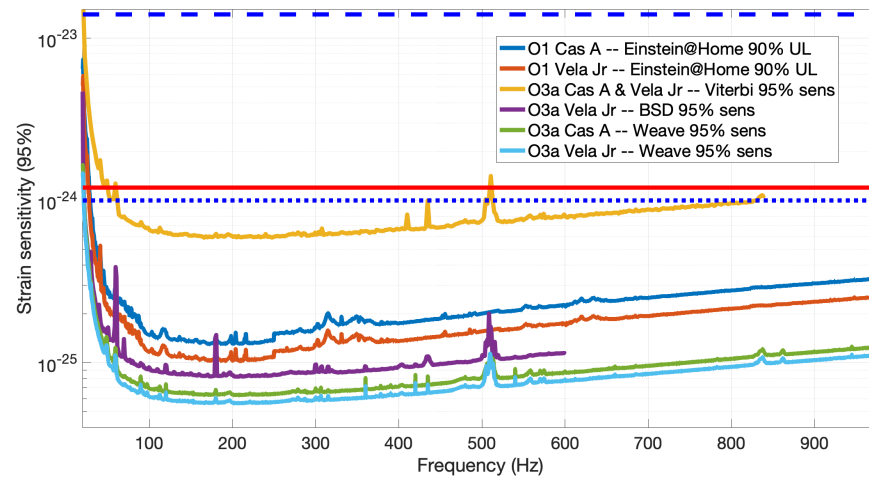
Searches for supernova remnants in LIGO-Virgo O3a data are reported in [247,248]. To date, the results in [247] are the most stringent for the source targeted: Cassiopeia A (Cas A, G111.7-2.1) and Vela Jr. (G266.2-1.2) supernova remnants. Both sources are extremely young, with inferred lower estimate ages of ∼300 years for Cas A, and ∼700 years for Vela Jr. With these assumptions, these targets have a corresponding indirect age-based limit (see Equation (12)) of ∼1.2×10^{-24} for the central compact object in Cas A, assuming a distance of 3.3 kpc, and 1.4×10^{-23} for Vela Jr. if located at 0.2 kpc. The search is based on the semi-coherent Weave method [159]. No GW signal is detected in the analyzed band, and the best sensitivity to the signal strain amplitude reached in this search is ∼6.3×10^{-26} for Cas A and ∼5.6×10^{-26} for Vela Jr., well below their age-based upper limit. A comparative plot is shown in Figure 3, showing the upper limits provided by the searches in [247–249]. In the search reported in [248], three complementary pipelines have been used: the Band-Sampled-Data directed pipeline, the single harmonic Viterbi and the dual harmonic Viterbi pipelines. Each pipeline used different signal models and methods for the identification of noise artifacts. In particular, the two Viterbi pipelines are robust to sources with spin wandering. This search targets a total of 15 supernova remnants, including Cas A, Vela Jr. and G347.3-0.5. These three targets have also been analyzed in a previous Einstein@Home search [250] using O1 data. The most interesting candidates of this search have been followed up in O2 data, along with new sub-threshold candidates of the same O1 search as reported in [249]. A full deep search for CWs from G347.3-0.5 in the frequency band below 400 Hz in O2 LIGO data is described in [251]. This choice is justified by the existence of a sub-threshold candidate at around 369 Hz that survived the search in [249]. The same candidate has been further investigated with an MCMC method in O2 data [205]. Any significant result has been reported from this search in O2 data, and hence, upper limits are provided, improving those from the same search in O1 data and those from the more robust single harmonic Viterbi tracker in O3a [248].

For the closest target Vela Jr., the best upper limit in [248] is 8.2×10^{-26} for the band-sampled-data pipeline. This result is more constraining than those set by [249,250]; however, it is less stringent than the results in [247] by a factor of 30% (see Figure 3). It should be noted that the searches in [249,250] used O1 and O2 data, while the searches in [247,248] used data from detectors with improved sensitivity (O3a). However, the Einstein@Home O1 searches [249,250] used a coherent integration duration ∼20–150 times longer than the one in the band-sampled-data search in [248], while the Weave search in [247] used a coherence length 10–70 times longer. This guarantees a starting theoretical sensitivity gain of a factor of 2.1–3.5 and 1.7–2.9 for [249,250] and [247], respectively[5]. On the other hand, the use of longer coherence times corresponds to an increase in the computing power needed for the search, as it scales at least as the fourth power of the coherence time. Furthermore, the use of a longer coherence time may negatively impact the robustness of the search. This makes it clear that different approaches are needed when wide parameter space searches are performed, choosing the right balance between computing cost, robustness and sensitivity.

Previous searches for CW from some of the 15 targets investigated in [248] are presented in [252,253] using LIGO O2 data, although using, respectively, a fully coherent

method and a less sensitive but model robust Viterbi tracker. A previous fully coherent O1 search is given in [254], also listing among the targets the extrasolar planet candidate Fomalhaut b suggested to be a nearby old NS. The latter is also investigated in [255] using a hidden Markov model Viterbi tracker.


Figure 3. Results taken from the supernova remnant search in LIGO O3a data for Cas A and Vela Jr using Weave [247]. Estimated GW strain amplitude sensitivities are given at the 95% confidence level. Additional results from prior searches for Cas A and Vela Jr. in O1 Einstein@Home 90% C.L. [250] and the O3a model-robust Viterbi method (yellow) and band-sampled-data method (purple) [248]. The solid red horizontal line indicates the age-based upper limit on the Cas A strain amplitude. The dashed (dotted) horizontal blue lines indicate the optimistic (pessimistic) age-based upper limit on Vela Jr. strain amplitude, assuming an age and distance of 700 yr and 0.2 kpc (5100 yr and 1.0 kpc). Figure adapted from [247].

4.1.3. Low-Mass X-ray Binaries and Sco-X1

A significant fraction of observed known NS is in a binary system. Among these, LMXBs are of particular interest for CW searches. Indeed, the presence of a GW torque could explain why the maximum observed spinning frequency 716 Hz for PSR J1748-2446ad is well below the centrifugal breakup frequency, estimated at ∼1400 Hz. These systems are typically formed by an NS (or stellar-mass BH) and a low mass ($\leq 1 M_\odot$) stellar companion. A recent search for CWs from 20 accreting millisecond X-ray pulsars in O3 data is given in [256]. Five of these twenty accreting pulsars have already been analyzed with the same method in O2 data [257]. The search relies on the EM observation of the spin frequencies and orbital parameters of the system, happening during the active outburst phase. The algorithm uses a hidden Markov model (implemented via Viterbi) to track spin wandering [170] and combines its results with the J -statistic to account for the orbital phase modulation [179]. For each target, the search looks for CW signals in sub-bands around $\{1, 4/3, 2\} f_{\text{spin}}$. One of the targets, SAX J1808.4-3658, went into outburst during O3a. Given that, according to some models, CWs are only emitted during this outburst phase [258], an opportunistic search for SAX J1808.4-3658 is also provided in [256]. No significant candidates are reported from this search. However, upper limits have been placed on the GW strain amplitude with 95% confidence level. The strictest constraint is 4.7×10^{-26} from IGR J17062-6143. The stringent constraints on the ellipticity for the $f_{\text{gw}} = 2 f_{\text{spin}}$ case is $\varepsilon^{95\%} = 3.1 \times 10^{-7}$ for the IGR J00291+5934 source. The corresponding upper limit on the r-mode amplitude ($f_{\text{gw}} = \frac{4}{3} f_{\text{spin}}$) is $\alpha^{95\%} = 1.8 \times 10^{-5}$ for the same source.

To date, several searches have targeted Sco X-1 [259–262] in advanced detector data. The latest results using O3 data are reported in [263]. Sco-X1 is a very interesting candidate for CW searches since it is the brightest extrasolar X-ray source in the sky, which means that it is potentially an optimal source of GWs [264,265]. The system is composed of a 1.4 $M_\odot$ NS and a 0.7 $M_\odot$ companion star [266]. Although being a known source, no EM measurement

of the rotation frequency and frequency derivative exists for Sco-X1. In addition to these uncertainties, some of the binary parameters are barely known, making the search for this source very computationally challenging. To date, no CW is reported for this source, while the torque-balance limit (see Equation (13)) has been beaten for the first time in [259], using CrossCorr method [178,267] in O2 data. The best constraints are as low as 7.06×10^{-26}, assuming an NS spin inclination $\iota = 44° \pm 6°$ [266,268]. To date, none of the searches beats the limit if an isotropic prior on ι is made, as reported in Figure 4. A different method has been used in the latest search for Sco-X1 in O3 [263], using a hidden Markov model pipeline implemented with the Viterbi algorithm [179]. This method, although being less sensitive than the cross-correlation search, provides a complementary tool to CrossCorr results. The upper limits from the O3 search are on average $\sim$3 times lower than those from the O2 hidden Markov model search [261] and 13 lower than the same search in O1 data [260]. Previous searches using O1 data and the hidden Markov model and CrossCorr methods are reported in [260,262]. In O3, the lowest $h_0^{95\%}$ for a hidden Markov model tracked signal are $4.56 \times 10^{-26}, 6.16 \times 10^{-26}$, and 9.41×10^{-26} for circular ($\iota = 0°$), electromagnetically restricted ($\iota = 44°$) and unknown polarizations, respectively. Furthermore, for the hidden Markov model search, the torque balance limit is beaten for a fixed ι below 200 Hz and for r_m equal to the NS radius or the Alfven radius [260]. By beating the torque balance limit for r_m at the Alfven radius, it is possible to identify some exclusion region over the mass-radius-magnetic field combination for some equation-of-state models (see [259] for a discussion). Constraints in the mass–radius plane are also possible when r_m equals the NS radius.
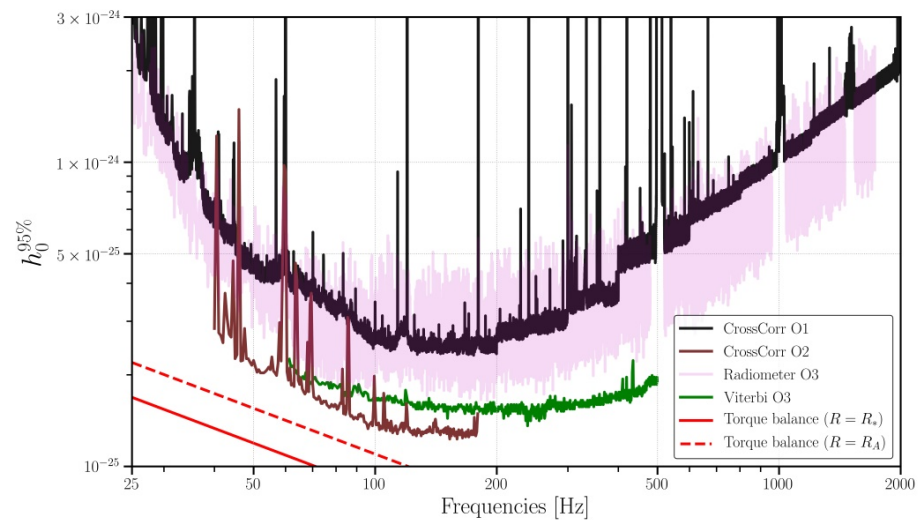

Figure 4. GW strain upper limits at 95% confidence as a function of frequency. No assumption on the ι angle is made for the curves in the figure. The curves are for the CrossCorr O1 search [262] (black line), the CrossCorr O2 search [259] (brown line), the Radiometer O3 search [269] (light pink line), and the O3 hidden Markov model search [263] (green line). The indirect torque-balance upper limits (see Equation (13)), for the $r_m = R$ case (red solid line) and for r_m equal to the Alfven radius (dashed red line), are also plotted. Figure taken from [263].

4.2. Results from Unknown Sources (All-Sky, Spotlight Surveys, Dark Matter Candidates)

In the absence of EM-driven information, wide parameter space searches for unknown sources allow scouring the whole sky in search for EM silent sources. These searches include all-sky surveys for isolated NS and NS in binary systems. It is also usual to look for CWs from a specific and over-populated region in the sky, such as the Galactic Center or some globular clusters. In these cases, sometimes the information provided by EM observations is not enough to shed light on the exact population of the analyzed region, and GWs could help in this direction. Finally, through GWs, we could also look for DM candidates.

4.2.1. All-Sky Surveys

The latest results for all-sky surveys using LIGO-Virgo O3 data are reported in [270] and a summary of the results can be found in Figure 5. Four different analysis methods are used to look for signals from isolated non-axisymmetric NSs: the FrequencyHough [151], Sky-Hough [154], Time-Domain F-statistic [140,157], and SOAP [176], and for the first time, applied in an all-sky CW search. The frequency investigated ranges from 10 to 2048 Hz and from -10^{-8} to 10^{-9} Hz/s for the first frequency derivative[6], each pipeline covers a subset of this parameter space except for the FrequencyHough. The frequency range is wide enough to cover most of the expected sources: young and energetic NS, millisecond pulsars and signals from r-mode oscillations. The search results are generic and are valid for any quasi-monochromatic, persistent signal characterized by the parameters investigated in this search following the linear phase evolution in Equation (29). Constraints on the rate and abundance of inspiraling planetary-mass and asteroid-mass PBHs are also discussed in this search. No GW observation has been reported, and the best constraint on the strain amplitude at the 95% confidence level is $\sim 1.1 \times 10^{-25}$ in the 100–200 Hz frequency range. This is the first all-sky search using Advanced Virgo data.
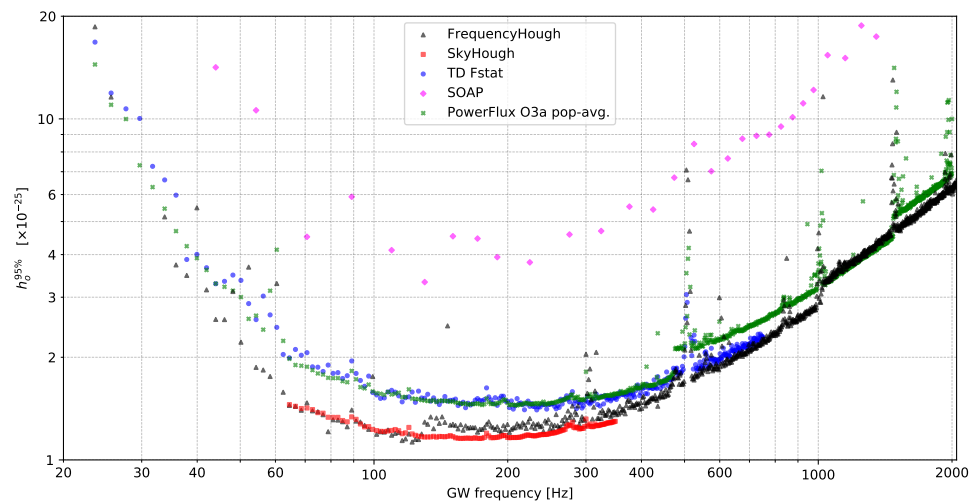
Figure 5. Comparison of 95% confidence upper limits on GW amplitude obtained in the O3 all-sky search by the FrequencyHough pipeline (black triangles), the SkyHough pipeline (red squares), the Time-Domain F-statistic pipeline (blue circles), and the SOAP pipeline (magenta diamonds). Population-averaged upper limits obtained in the Powerflux O3a search are marked with dark-green crosses. Figure taken from [161].

A previous search using the PowerFlux pipeline on O3a data [161] provided an upper limit on the strain, for the most favorable orientation, of 6.3×10^{-26}, improving previous results from O2 data. If compared with the population-averaged upper limit, the lowest 95% C.L. in O3a is 1.4×10^{-25}, less constraining than the full O3 search in [270] (see Figure 5). Results from this search have been used to constrain the rate and abundance of inspiraling PBHs in [271]. To date, only the O2 Falcon search beats the upper limits in [270], although the frequency derivative range is at least 10^3 smaller, making the results in [270], de facto, the most stringent limits for sources with spin-down as low as -1×10^{-8} Hz/s in the 20–2000 Hz frequency range.

Upper limits on the ellipticity are also derived in [270]. The search is able to detect nearby sources, within 100 pc, with ellipticities above 3×10^{-7} emitting at 200 Hz, or even ellipticities as low as $\sim 2 \times 10^{-9}$ for sources spinning at the highest frequencies. For sources located as far as the Galactic Center region (8–10 kpc), the search is able to detect signals with ellipticities bigger than $\sim 3 \times 10^{-6}$ for frequencies above 1500 Hz. Probing very small ellipticities with such a wide parameter space search certainly goes in the right direction for a detection. Indeed, ellipticities below 10^{-7} are in the expected range of sustainable

strains in NS crusts [58,60,62–64]. Previous searches performed using O2 data are given in [272–276], and O1 searches can be found in [277–279].

No CW detection is reported from all-sky searches for unknown NSs in binary systems. The latest search, carried out on O3a data [280,281], placed upper limits on the strain at 2.4×10^{-25} for NSs in binary systems spanning orbital periods of 3–45 days. The search, carried out using the BinarySkyHough pipeline in O3a, is the update of the O2 all-sky binary survey presented in [282], reporting an improved result by a factor of 1.6. A good fraction of known NS is in a binary system. Despite this, no other all-sky search, specifically tailored for unknown binaries, has been carried out in advanced detector data. The main reason for this lack is due to the huge computing cost associated with these searches, significantly overcoming the already computationally demanding all-sky searches for isolated NS. However, according to [283], for some combinations of the binary period and semi-major axis parameters, results from wide parameter space searches for unknown isolated sources are also valid for the binary case.

4.2.2. Spotlight Surveys: The Galactic Center and Terzan 5

Directed searches targeting interesting sky regions such as the Galactic Center and the globular cluster Terzan 5 have been carried out in advanced detector data. Indeed, concerning the Galactic Center, a significant population of up to hundreds or even thousands of NSs is expected to exist [284,285]. Moreover, the true composition of this region, showing an extended gamma-ray emission from its center [286–288], is still under debate and could be explained, for instance, by the presence of an unresolved population of millisecond pulsars [289–293]. A recent search for the CW emission from the Galactic center region has been carried out in O3 LIGO and Virgo data [294]. The search uses a semi-coherent method developed in the band-sampled data framework and span a wider parameter space compared to the previous O2 search in [295]. The frequency investigated ranges from 10 Hz to 2000 Hz, while the spin-down/up lies between $[-1.8 \times 10^{-8}; 10^{-10}]$ Hz/s. No CW signal has been detected, and upper limits on the GW amplitude are presented. To date, this search reports the most stringent upper limit for targets located within 30–300 parsecs from the Galactic Center, with a minimum strain of $\sim 7.6 \times 10^{-26}$ at 142 Hz at a 95% confidence level. The same search reports upper limits on the ellipticity and the r-mode amplitude. The same search has been used to identify exclusion regions in the BH/boson cloud mass plane for sources located in the Galactic Center.

A previous search for CW from the Galactic Center and Terzan 5 is reported in [296] using O1 data. The search, based on a loosely coherent method, looks for signals emitting at frequencies in the range $[475; 1500]$ Hz and with frequency time derivatives in the range $[-3.0; 0.1] \times 10^{-8}$ Hz/s. O3 data have already been used to make a lower sensitivity search for an unresolved GW emission from the Galactic Center region using stochastic GW search methods [269].

4.2.3. Dark Matter Candidates—Ultralight Bosons and CDOs

Methods for the search of CW from NSs can be easily adapted to any kind of GW signal with features similar to the standard NS case. An emerging family of searches is the one for DM candidates. This branch of investigations through CW tools is very immature when compared, e.g., with known pulsars searches. Nevertheless, some searches have been carried out in advanced detector data. In Section 2.2, the major DM systems investigated in CW searches have been described: boson clouds around spinning BHs, ultralight vector bosons and CDOs.

The first all-sky survey for persistent, quasi-monochromatic GW signals emitted by ultralight scalar boson clouds around spinning BHs is reported in [297]. The search analyzed the frequency range $[20; 610]$ Hz of the O3 observing run of Advanced LIGO. According to the expected spin wandering signal model from boson clouds, a small range around the $\dot{f}_{\mathrm{gw}}$ parameter has been considered. The main search has been carried out using the method in [194], and the most interesting candidates have been followed up with

a FrequencyHough-based method and the Viterbi method. No potential CW candidate remains after the follow-up, and upper limits on the signal strain are provided at the 95% confidence level. The minimum value is 1.04×10^{-25} in the most sensitive frequency region of the detectors $\sim$130 Hz. These upper limits on the strain can be translated into exclusion regions in the BH-boson cloud mass plane after assuming some parameters of the BH population: the age of the source, its distance and its spin. Along with these exclusion regions, it is possible to derive the maximum distance at which a given BH-boson cloud system, with a certain age, is not emitting CWs, as a function of the boson mass (see Figure 6). In other words, these maximum distances tell us how far we can exclude the presence of an emitting system according to the null detection results obtained by the search. These constraints have been computed by simulating a BH population with masses in the range $[5; 100]$ $M_\odot$ and a uniform spin distribution in the range $[0.2; 0.9]$. The maximum distance corresponds to the distance at which at least 5% of the simulated signal produces a strain amplitude higher than the upper limits of the search, meaning that it would have been detected. The paper in [297] also reports the same figure but for a BH population with maximum masses of 50 $M_\odot$. These constraints strongly depend on the ensemble properties of the simulated BH population. The plot in Figure 6 shows that the presence of systems younger than 10^3 yrs is disfavored within the Galaxy, if formed by bosons with masses above 1.2×10^{-13} eV, for the considered BH mass distribution. Older systems, which produce a smaller strain amplitude, are more difficult to constrain.
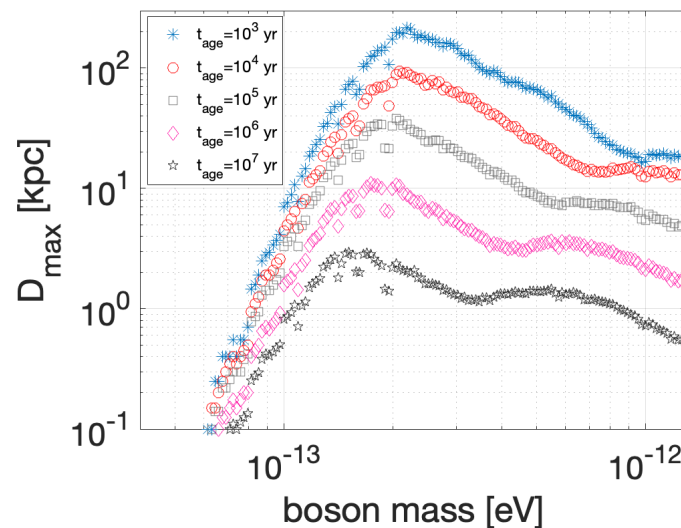
Figure 6. Maximum distance at which at least 5% of a simulated population of BHs-boson cloud would produce a detectable GW signal in the search described in [297]. The simulated population has a maximum BH mass of $100 M_\odot$. The curve is produced for different markers for systems with ages between 10^3 yrs and 10^7 yrs, as indicated in the legend. Figure taken from [297].

The search in [297] is the first of this type, all-sky type and optimized for frequency wandering signals, although it is possible to compute the same exclusion regions of the BH/scalar boson mass parameter space also using upper limits from all-sky searches for spinning NSs as in [100]. A previous directed search for boson clouds from Cygnus X-1 was performed in O2 data in [298] using the same Markov model Viterbi method applied for the follow-up of the all-sky boson cloud O3 search [297].

Another potential candidate for CW signals, in the subset of the ultralight DM particles with masses 10^{-14}–10^{-11} eV/c^2 is a vector boson, the dark photon, which directly couples to GW interferometers (see Section 2.2). The latest O3 LIGO-Virgo data all-sky search for the CW signature from this type of system provided in [123]. The boson mass range probed by this search is $(2$–$4) \times 10^{-13}$ eV/c^2, corresponding to the detectors frequencies $[10; 2000]$ Hz. The search applies two complementary methods. One pipeline is based on a cross-correlation method [106] and already used in a previous dark photon DM O1

search [117]. The second is a semi-coherent method [196] based on the band-sampled-data framework [147] and adapted from the one used in the latest O3 BH-boson cloud search [194,297]. No evidence of DM signatures has been found, and upper limits on the signal strain are derived. These limits can be converted into upper limits on the coupling factor of the interaction between the dark photon and the baryons in the detector. These constraints surpass the ones provided by existing DM experiments, such as the Eöt–Wash torsion balance [299] and MICROSCOPE [300], and improve previous O1 results by a factor ∼100.

Searches for CW signatures from a pair of CDOs or PBHs far from the coalescence are also possible. The only actual search for systems with a frequency and amplitude evolution described by Equations (25) and (26) has been performed in O1 data [124]. How these CDOs can be formed is still under debate. One option is to assume that these objects can be trapped by normal matter, for instance a planet or even the Sun. Once these objects are formed, binaries can form if orbiting close enough to each other. CDOs emitting GWs from the inspiral phase inside a solar system object should be very dense and in a very close binary orbit. The search in [124] searches for CW signals from CDOs orbiting near the center of the Sun in the GW frequency range 50–550 Hz. No signal is claimed, and upper limits are provided. These limits are converted into upper limits on the mass of CDOs. For almost the full frequency range investigated, these limits are below 10^{-9} $M_\odot$ with a minimum value of 5.8×10^{-10} $M_\odot$ at 525.5 Hz.

Constraints on the rates and abundances of nearby planetary- and asteroid-mass primordial BHs are provided in [270,271]. These constraints are mapped from the upper limits strain results of the O3a Powerflux search and the O3 FrequencyHough search with minimal modeling assumptions on the PBH population. As anticipated in the previous paragraph, the search in [270] targets CW from unknown NS, but the results can be generalized for the case of CDOs or PBHs far from the coalescence as far as they follow a linear frequency evolution. In principle, this search is able to probe GW signals below 250 Hz from inspiralling PBHs binaries with chirp masses smaller than $O(10^{-5})M_\odot$. The constraints obtained from the latest full O3 search in [270] are more stringent than those presented in [271] from the O3a search thanks to the use of a longer observing time. Unfortunately, none of these results are stringent enough to be able to constrain the merging rate of PBHs but will certainly be interesting for future third-generation of detectors [301,302].

5. Conclusions

In recent years, we have witnessed the huge impact that GW science had on our understanding of the Universe. Each detection has provided an interesting tool to test what already is known, but mostly the unknown, about these fascinating compact objects able to emit GWs. The main actors in these scenes have been the well-known merger events, either as a pair of BHs or a system involving at least one NS. We have witnessed the birth of the so-called multi-messenger astronomy, an incredibly powerful way to depict the details of a binary NS merger through EM, neutrino and particle astronomy. However, this is just the beginning, and indeed, the increase in the detectors' sensitivity, expected for the upcoming fourth observing run, along with the improvement of existing pipelines, will certainly bring about the discovery of even more fascinating and unexpected phenomena. In this scenario, CW signals can be the next surprise in GW astronomy. A CW detection from NS could provide evidence for star deformations and shed light on the NS structure and their thermal, spin, and magnetic field evolution. On the other hand, if the CW detection happens to be in the case of a DM candidate such as from a boson cloud around spinning BH, this will lead to the first direct evidence of the existence of DM, solving one of the most intriguing open problems of astrophysics.

Unfortunately, to date, any search has been able to find strong evidence of GW emission from CW sources. However, an increasing number of known pulsars is surpassing their spin-down limit. The lowest constraints on the equatorial ellipticities are very close to realistic expectations for normal EOS. A comment is probably necessary to explain why,

even using the most sensitive pipelines for CW searches, any GW has been observed from these sources. It is not unlikely that the assumed models are not well representative of the realistic emission scenario happening for CW, in particular for NS. This is the main reason why, along with improvements in the pipeline's sensitivity, many approaches tend to improve the pipeline's robustness with respect to the model. The final answer to this long-debated issue of the existence (or not) of CW signals is probably just around the corner, and the upcoming O4 run is expected from a wide community of scientists to finally solve this unanswered question. Even if no detection happens during O4, a new generation of detectors—Einstein Telescope, Cosmic Explorer, LISA and more [301–306]—will start their observation in the future, providing even more interesting detection scenarios.

Conflicts of Interest: The author declares no conflict of interest.

Notes

1   Given the proportionality between f_{gw} and f_{spin}, here f can indicate any of the two frequencies.

2   for $m = 1$ and for $\alpha \ll 0.1$.

3   Hence, the time derivative of the time component of A_μ is negligible relative to $\vec{A}$.

4   Recycled pulsars are ordinary pulsars that have been spun up by accretion from a companion star in a binary system.

5   The ranges are due to fact that the coherence time used in [248] changes in each 10Hz frequency band.

6   except for the SOAP pipeline that covers the additional small region $[1000; 2048]$ Hz in frequency and $[10^{-9}; 10^{-8}]$ Hz/s in spin-up.

References

1. Aasi, J.; Abbott, B.P.; Abbott, R.; Abbott, T.; Abernathy, M.R.; Ackley, K.; Adams, C.; Adams, T.; Addesso, P.; Adhikari, R.X.; et al. Advanced LIGO. *Class. Quantum Gravity* **2015**, *32*, 074001. [CrossRef]

2. Acernese, F.; Agathos, M.; Agatsuma, K.; Aisa, D.; Allemandou, N.; Allocca, A.; Amarni, J.; Astone, P.; Balestri, G.; Ballardin, G.; et al. Advanced Virgo: A second-generation interferometric gravitational wave detector. *Class. Quantum Gravity* **2014**, *32*, 024001. [CrossRef]

3. Nardecchia, I. Detecting Gravitational Waves with Advanced Virgo. *Galaxies* **2022**, *10*, 28. [CrossRef]

4. Abbott, B.P.; Abbott, R.; Abbott, T.; Abraham, S.; Acernese, F.; Ackley, K.; Adams, C.; Adhikari, R.X.; Adya, V.B.; Affeldt, C.; et al. GWTC-1: A Gravitational-Wave Transient Catalog of Compact Binary Mergers Observed by LIGO and Virgo during the First and Second Observing Runs. *Phys. Rev. X* **2019**, *9*, 031040. [CrossRef]

5. Abbott, R.; Abbott, T.D.; Abraham, S.; Acernese, F.; Ackley, K.; Adams, A.; Adams, C.; Adhikari, R.X.; Adya, V.B.; Affeldt, C.; et al. GWTC-2: Compact Binary Coalescences Observed by LIGO and Virgo during the First Half of the Third Observing Run. *Phys. Rev. X* **2021**, *11*, 021053. [CrossRef]

6. The LIGO Scientific Collaboration; Abbott, R.; Abbott, T.D.; Acernese, F.; Ackley, K.; Adams, C.; Adhikari, N.; Adhikari, R.X.; Adya, V.B.; Affeldt, C.; et al. GWTC-2.1: Deep Extended Catalog of Compact Binary Coalescences Observed by LIGO and Virgo During the First Half of the Third Observing Run. *arXiv* **2021**, arXiv:2108.01045.

7. Abbott, R.; Abbott, T.D.; Acernese, F.; Ackley, K.; Adams, C.; Adhikari, N.; Adhikari, R.X.; Adya, V.B.; Affeldt, C.; Agarwal, D.; et al. GWTC-3: Compact Binary Coalescences Observed by LIGO and Virgo during the Second Part of the Third Observing Run. *arXiv* **2021** , arXiv:2111.03606.

8. Akutsu, T.; Ando, M.; Arai, K.; Arai, Y.; Araki, S.; Araya, A.; Aritomi, N.; Asada, H.; Aso, Y.; Atsuta, S.; et al. KAGRA: 2.5 generation interferometric gravitational wave detector. *Nat. Astron.* **2019**, *3*, 35–40. [CrossRef]

9. Di Giovanni, F.; Sanchis-Gual, N.; Cerdá-Durán, P.; Zilhão, M.; Herdeiro, C.; Font, J.A.; Radu, E. Dynamical bar-mode instability in spinning bosonic stars. *Phys. Rev. D* **2020**, *102*, 124009. [CrossRef]

10. Sanchis-Gual, N.; Di Giovanni, F.; Zilhão, M.; Herdeiro, C.; Cerdá-Durán, P.; Font, J.A.; Radu, E. Nonlinear Dynamics of Spinning Bosonic Stars: Formation and Stability. *Phys. Rev. Lett.* **2019**, *123*, 221101. [CrossRef]

11. DeMarchi, L.; Sanders, J.R.; Levesque, E.M. Prospects for Multimessenger Observations of Thorne-Zytkow Objects. *Astrophys. J.* **2021**, *911*, 101. [CrossRef]

12. Tenorio, R.; Keitel, D.; Sintes, A.M. Search Methods for Continuous Gravitational-Wave Signals from Unknown Sources in the Advanced-Detector Era. *Universe* **2021**, *7*, 474. [CrossRef]

13. Jones, D.I. Learning from the Frequency Content of Continuous Gravitational Wave Signals. *arXiv* **2021**, arXiv:2111.08561.
14. Sieniawska, M.; Bejger, M. Continuous Gravitational Waves from Neutron Stars: Current Status and Prospects. *Universe* **2019**, *5*, 217. [CrossRef]
15. Glampedakis, K.; Gualtieri, L. *Gravitational Waves from Single Neutron Stars: An Advanced Detector Era Survey*; Astrophysics and Space Science Library; Springer: Berlin/Heidelberg, Germany, 2018; pp. 673–736. [CrossRef]
16. Riles, K. Recent searches for continuous gravitational waves. *Mod. Phys. Lett. A* **2017**, *32*, 1730035. [CrossRef]
17. Lasky, P.D. Gravitational Waves from Neutron Stars: A Review. *Publ. Astron. Soc. Aust.* **2015**, *32*, e034. [CrossRef]
18. Bersanetti, D.; Patricelli, B.; Piccinni, O.J.; Piergiovanni, F.; Salemi, F.; Sequino, V. Advanced Virgo: Status of the Detector, Latest Results and Future Prospects. *Universe* **2021**, *7*, 322. [CrossRef]
19. Caudill, S.; Kandhasamy, S.; Lazzaro, C.; Matas, A.; Sieniawska, M.; Stuver, A.L. Gravitational-wave searches in the era of Advanced LIGO and Virgo. *Mod. Phys. Lett. A* **2021**, *36*, 2130022. [CrossRef]
20. Lattimer, J.M.; Prakash, M. The Physics of Neutron Stars. *Science* **2004**, *304*, 536–542. [CrossRef]
21. Haensel, P.; Potekhin, A.Y.; Yakovlev, D.G. *Neutron Stars 1: Equation of State and Structure*; Springer: New York, NY, USA, 2007; Volume 326. [CrossRef]
22. Duncan, R.C.; Thompson, C. Formation of Very Strongly Magnetized Neutron Stars: Implications for Gamma-Ray Bursts. *Astrophys. J. Lett.* **1992**, *392*, L9. [CrossRef]
23. Esposito, P.; Rea, N.; Israel, G.L. Magnetars: A Short Review and Some Sparse Considerations. In *Timing Neutron Stars: Pulsations, Oscillations and Explosions*; Astrophysics and Space Science Library; Springer: Berlin/Heidelberg, Germany, 2020; pp. 97–142. [CrossRef]
24. Haskell, B.; Sedrakian, A. Superfluidity and Superconductivity in Neutron Stars. In *The Physics and Astrophysics of Neutron Stars*; Astrophysics and Space Science Library; Springer: Berlin/Heidelberg, Germany, 2018; pp. 401–454. [CrossRef]
25. Chamel, N. Superfluidity and Superconductivity in Neutron Stars. *J. Astrophys. Astron.* **2017**, *38*, 43. s12036-017-9470-9. [CrossRef]
26. Baym, G.; Hatsuda, T.; Kojo, T.; Powell, P.D.; Song, Y.; Takatsuka, T. From hadrons to quarks in neutron stars: A review. *Rep. Prog. Phys.* **2018**, *81*, 056902. [CrossRef] [PubMed]
27. Oertel, M.; Hempel, M.; Klähn, T.; Typel, S. Equations of state for supernovae and compact stars. *Rev. Mod. Phys.* **2017**, *89*, 015007. [CrossRef]
28. Stone, J.R. Nuclear Physics and Astrophysics Constraints on the High Density Matter Equation of State. *Universe* **2021**, *7*, 257. [CrossRef]
29. Burgio, G.; Schulze, H.J.; Vidaña, I.; Wei, J.B. Neutron stars and the nuclear equation of state. *Prog. Part. Nucl. Phys.* **2021**, *120*, 103879. [CrossRef]
30. Annala, E.; Gorda, T.; Kurkela, A.; Nättilä, J.; Vuorinen, A. Evidence for quark-matter cores in massive neutron stars. *Nat. Phys.* **2020**, *16*, 907–910. [CrossRef]
31. Vidaña, I. Hyperons: The strange ingredients of the nuclear equation of state. *Proc. R. Soc. A Math. Phys. Eng. Sci.* **2018**, *474*, 20180145. [CrossRef]
32. Pethick, C.J.; Schaefer, T.; Schwenk, A. Bose-Einstein condensates in neutron stars. *arXiv* **2015**, arXiv:1507.05839.
33. Baym, G.; Flowers, E. Pion condensation in neutron star matter: Equilibrium conditions and model calculations. *Nucl. Phys. A* **1974**, *222*, 29–64. [CrossRef]
34. Ramos, A.; Schaffner-Bielich, J.; Wambach, J. Kaon Condensation in Neutron Stars. In *Physics of Neutron Star Interiors*; Lecture Notes in Physics; Blaschke, D., Sedrakian, A., Glendenning, N.K., Eds.; Springer: Berlin/Heidelberg, Germany, 2001; Volume 578. [CrossRef]
35. Özel, F.; Freire, P. Masses, Radii, and the Equation of State of Neutron Stars. *Annu. Rev. Astron. Astrophys.* **2016**, *54*, 401–440. [CrossRef]
36. Watts, A.L.; Andersson, N.; Chakrabarty, D.; Feroci, M.; Hebeler, K.; Israel, G.; Lamb, F.K.; Miller, M.C.; Morsink, S.; Özel, F.; et al. Colloquium: Measuring the neutron star equation of state using x-ray timing. *Rev. Mod. Phys.* **2016**, *88*, 021001. [CrossRef]
37. Steiner, A.W.; Lattimer, J.M.; Brown, E.F. The neutron star mass-radius relation and the equation of state of dense matter. *Astrophys. J.* **2013**, *765*, L5. [CrossRef]
38. Lattimer, J.M. Neutron star masses and radii. *AIP Conf. Proc.* **2019**, *2127*, 020001. [CrossRef]
39. Llanes-Estrada, F.J.; Lope-Oter, E. Hadron matter in neutron stars in view of gravitational wave observations. *Prog. Part. Nucl. Phys.* **2019**, *109*, 103715. [CrossRef]
40. Bogdanov, S.; Lamb, F.K.; Mahmoodifar, S.; Miller, M.C.; Morsink, S.M.; Riley, T.E.; Strohmayer, T.E.; Tung, A.K.; Watts, A.L.; Dittmann, A.J.; et al. Constraining the Neutron Star Mass–Radius Relation and Dense Matter Equation of State with NICER. II. Emission from Hot Spots on a Rapidly Rotating Neutron Star. *Astrophys. J.* **2019**, *887*, L26. [CrossRef]
41. Cromartie, H.T.; Fonseca, E.; Ransom, S.M.; Demorest, P.B.; Arzoumanian, Z.; Blumer, H.; Brook, P.R.; DeCesar, M.E.; Dolch, T.; Ellis, J.A.; et al. Relativistic Shapiro delay measurements of an extremely massive millisecond pulsar. *Nat. Astron.* **2019**, *4*, 72–76. [CrossRef]
42. Guillot, S.; Rutledge, R.E. Rejecting proposed dense matter equations of state with Quiescent low-mass X-ray binaries. *Astrophys. J.* **2014**, *796*, L3. [CrossRef]
43. Nattila, J.; Miller, M.C.; Steiner, A.W.; Kajava, J.J.E.; Suleimanov, V.F.; Poutanen, J. Neutron star mass and radius measurements from atmospheric model fits to X-ray burst cooling tail spectra. *Astron. Astrophys.* **2017**, *608*, A31. [CrossRef]

44. Wei, J.B.; Figura, A.; Burgio, G.F.; Chen, H.; Schulze, H.J. Neutron star universal relations with microscopic equations of state. *J. Phys. G Nucl. Part. Phys.* **2019**, *46*, 034001. [CrossRef]

45. Gendreau, K.; Arzoumanian, Z. Searching for a pulse. *Nat. Astron.* **2017**, *1*, 895–895. [CrossRef]

46. Miller, M.C.; Lamb, F.K.; Dittmann, A.J.; Bogdanov, S.; Arzoumanian, Z.; Gendreau, K.C.; Guillot, S.; Harding, A.K.; Ho, W.C.G.; Lattimer, J.M.; et al. PSR J0030+0451 Mass and Radius from NICER Data and Implications for the Properties of Neutron Star Matter. *Astrophys. J.* **2019**, *887*, L24. [CrossRef]

47. Abbott, B.; Abbott, R.; Abbott, T.; Acernese, F.; Ackley, K.; Adams, C.; Adams, T.; Addesso, P.; Adhikari, R.; Adya, V.; et al. GW170817: Observation of Gravitational Waves from a Binary Neutron Star Inspiral. *Phys. Rev. Lett.* **2017**, *119*, 161101. [CrossRef] [PubMed]

48. Abbott, B.P.; Abbott, R.; Abbott, T.D.; Acernese, F.; Ackley, K.; Adams, C.; Adams, T.; Addesso, P.; Adhikari, R.X.; Adya, V.B.; et al. Gravitational Waves and Gamma-Rays from a Binary Neutron Star Merger: GW170817 and GRB 170817A. *Astrophys. J.* **2017**, *848*, L13. [CrossRef]

49. Abbott, B.P.; Abbott, R.; Abbott, T.D.; Acernese, F.; Ackley, K.; Adams, C.; Adams, T.; Addesso, P.; Adhikari, R.X.; Adya, V.B.; et al. Multi-messenger Observations of a Binary Neutron Star Merger. *Astrophys. J.* **2017**, *848*, L12. [CrossRef]

50. Abbott, B.; Abbott, R.; Abbott, T.; Acernese, F.; Ackley, K.; Adams, C.; Adams, T.; Addesso, P.; Adhikari, R.; Adya, V.; et al. GW170817: Measurements of Neutron Star Radii and Equation of State. *Phys. Rev. Lett.* **2018**, *121*, 161101. [CrossRef]

51. Abbott, B.P.; Abbott, R.; Abbott, T.D.; Abraham, S.; Acernese, F.; Ackley, K.; Adams, C.; Adhikari, R.X.; Adya, V.B.; Affeldt, C.; et al. GW190425: Observation of a Compact Binary Coalescence with Total Mass 3.4 $M_\odot$. *Astrophys. J. Lett.* **2020**, *892*, L3. [CrossRef]

52. Abbott, R.; Abbott, T.D.; Abraham, S.; Acernese, F.; Ackley, K.; Adams, C.; Adhikari, R.X.; Adya, V.B.; Affeldt, C.; Agathos, M.; et al. GW190814: Gravitational Waves from the Coalescence of a 23 Solar Mass Black Hole with a 2.6 Solar Mass Compact Object. *Astrophys. J. Lett.* **2020**, *896*, L44. [CrossRef]

53. Abbott, R.; Abbott, T.D.; Abraham, S.; Acernese, F.; Ackley, K.; Adams, A.; Adams, C.; Adhikari, R.X.; Adya, V.B.; Affeldt, C.; et al. Observation of Gravitational Waves from Two Neutron Star–Black Hole Coalescences. *Astrophys. J. Lett.* **2021**, *915*, L5. [CrossRef]

54. Cerda-Duran, P.; Elias-Rosa, N. Neutron Stars Formation and Core Collapse Supernovae. In *The Physics and Astrophysics of Neutron Stars*; Astrophysics and Space Science Library; Springer: Berlin/Heidelberg, Germany, 2018; pp. 1–56. [CrossRef]

55. Baiotti, L.; Rezzolla, L. Binary neutron star mergers: A review of Einstein's richest laboratory. *Rep. Prog. Phys.* **2017**, *80*, 096901. [CrossRef]

56. Haskell, B.; Schwenzer, K. Isolated Neutron Stars. In *Handbook of Gravitational Wave Astronomy*; Bambi, C., Katsanevas, S., Kokkotas, K.D., Eds.; Springer: Singapore, 2021. [CrossRef]

57. Shapiro, S.L.; Teukolsky, S.A. *Black Holes, White Dwarfs, and Neutron Stars: The Physics of Compact Objects*; Wiley: Weinheim, Germany, 1983.

58. Ushomirsky, G.; Cutler, C.; Bildsten, L. Deformations of accreting neutron star crusts and gravitational wave emission. *Mon. Not. R. Astron. Soc.* **2002**, *319*, 902–932. [CrossRef]

59. Owen, B.J. Maximum Elastic Deformations of Compact Stars with Exotic Equations of State. *Phys. Rev. Lett.* **2005**, *95*, 211101. [CrossRef] [PubMed]

60. Johnson-McDaniel, N.K.; Owen, B.J. Maximum elastic deformations of relativistic stars. *Phys. Rev. D* **2013**, *88*, 044004. [CrossRef]

61. Woan, G.; Pitkin, M.D.; Haskell, B.; Jones, D.I.; Lasky, P.D. Evidence for a Minimum Ellipticity in Millisecond Pulsars. *Astrophys. J.* **2018**, *863*, L40. [CrossRef]

62. Gittins, F.; Andersson, N.; Jones, D.I. Modelling neutron star mountains. *Mon. Not. R. Astron. Soc.* **2020**, *500*, 5570–5582. [CrossRef]

63. Gittins, F.; Andersson, N. Modelling neutron star mountains in relativity. *Mon. Not. R. Astron. Soc.* **2021**, *507*, 116–128. [CrossRef]

64. Haskell, B.; Jones, D.I.; Andersson, N. Mountains on Neutron Stars: Accreted versus Non-Accreted Crusts. *Mon. Not. R. Astron. Soc.* **2006**, *373*, 1423–1439. Available online: https://academic.oup.com/mnras/article-pdf/373/4/1423/11177018/mnras0373-1423.pdf (accessed on 2 May 2022). [CrossRef]

65. Horowitz, C.J.; Kadau, K. Breaking Strain of Neutron Star Crust and Gravitational Waves. *Phys. Rev. Lett.* **2009**, *102*, 191102. [CrossRef]

66. Mastrano, A.; Melatos, A.; Reisenegger, A.; Akgün, T. Gravitational Wave Emission from a Magnetically Deformed Non-Barotropic Neutron Star. *Mon. Not. R. Astron. Soc.* **2011**, *417*, 2288–2299. Available online: https://academic.oup.com/mnras/article-pdf/417/3/2288/3826519/mnras0417-2288.pdf (accessed on 2 May 2022). [CrossRef]

67. Suvorov, A.G.; Mastrano, A.; Geppert, U. Gravitational Radiation from Neutron Stars Deformed by Crustal Hall Drift. *Mon. Not. R. Astron. Soc.* **2016**, *459*, 3407–3418. Available online: https://academic.oup.com/mnras/article-pdf/459/3/3407/8110424/stw909.pdf (accessed on 2 May 2022). [CrossRef]

68. Haskell, B.; Samuelsson, L.; Glampedakis, K.; Andersson, N. Modelling Magnetically Deformed Neutron Stars. *Mon. Not. R. Astron. Soc.* **2008**, *385*, 531–542. Available online: https://academic.oup.com/mnras/article-pdf/385/1/531/3465601/mnras0385-0531.pdf (accessed on 2 May 2022). [CrossRef]

69. Owen, B.J.; Lindblom, L.; Cutler, C.; Schutz, B.F.; Vecchio, A.; Andersson, N. Gravitational waves from hot young rapidly rotating neutron stars. *Phys. Rev. D* **1998**, *58*, 084020. [CrossRef]

70. Lindblom, L.; Owen, B.J.; Morsink, S.M. Gravitational Radiation Instability in Hot Young Neutron Stars. *Phys. Rev. Lett.* **1998**, *80*, 4843–4846. [CrossRef]

71. Kokkotas, K.D.; Schwenzer, K. r-mode astronomy. *Eur. Phys. J. A* **2016**, *52*, 38. [CrossRef]
72. Owen, B.J. How to adapt broad-band gravitational-wave searches for *r*-modes. *Phys. Rev. D* **2010**, *82*, 104002. [CrossRef]
73. Lockitch, K.H.; Friedman, J.L.; Andersson, N. Rotational modes of relativistic stars: Numerical results. *Phys. Rev. D* **2003**, *68*, 124010. [CrossRef]
74. Idrisy, A.; Owen, B.J.; Jones, D.I. R-mode frequencies of slowly rotating relativistic neutron stars with realistic equations of state. *Phys. Rev. D* **2015**, *91*, 024001. [CrossRef]
75. Caride, S.; Inta, R.; Owen, B.J.; Rajbhandari, B. How to search for gravitational waves from *r*-modes of known pulsars. *Phys. Rev. D* **2019**, *100*, 064013. [CrossRef]
76. Watts, A.L.; Krishnan, B.; Bildsten, L.; Schutz, B.F. Detecting gravitational wave emission from the known accreting neutron stars. *Mon. Not. R. Astron. Soc.* **2008**, *389*, 839–868. [CrossRef]
77. Haskell, B.; Zdunik, J.L.; Fortin, M.; Bejger, M.; Wijnands, R.; Patruno, A. Fundamental physics and the absence of sub-millisecond pulsars. *Astron. Astrophys.* **2018**, *620*, A69. [CrossRef]
78. Gittins, F.; Andersson, N. Population synthesis of accreting neutron stars emitting gravitational waves. *Mon. Not. R. Astron. Soc.* **2019**, *488*, 99–110. [CrossRef]
79. Andersson, N.; Glampedakis, K.; Haskell, B.; Watts, A.L. Modelling the Spin Equilibrium of Neutron Stars in Low-Mass X-ray Binaries without Gravitational Radiation. *Mon. Not. R. Astron. Soc.* **2005**, *361*, 1153–1164. Available online: https://academic.oup.com/mnras/article-pdf/361/4/1153/3885817/361-4-1153.pdf (accessed on 2 May 2022). [CrossRef]
80. Mukherjee, A.; Messenger, C.; Riles, K. Accretion-induced spin-wandering effects on the neutron star in Scorpius X-1: Implications for continuous gravitational wave searches. *Phys. Rev. D* **2018**, *97*, 043016. [CrossRef]
81. Leaci, P.; Astone, P.; D'Antonio, S.; Frasca, S.; Palomba, C.; Piccinni, O.; Mastrogiovanni, S. Novel directed search strategy to detect continuous gravitational waves from neutron stars in low- and high-eccentricity binary systems. *Phys. Rev. D* **2017**, *95*, 122001. [CrossRef]
82. Yim, G.; Jones, D.I. Transient Gravitational Waves from Pulsar Post-Glitch Recoveries. *Mon. Not. R. Astron. Soc.* **2020**, *498*, 3138–3152. Available online: https://academic.oup.com/mnras/article-pdf/498/3/3138/33780576/staa2534.pdf (accessed on 2 May 2022). [CrossRef]
83. Palomba, C. Simulation of a population of isolated neutron stars evolving through the emission of gravitational waves. *Mon. Not. R. Astron. Soc.* **2005**, *359*, 1150–1164. [CrossRef]
84. Jones, D.I. Gravitational wave emission from rotating superfluid neutron stars. *Mon. Not. R. Astron. Soc.* **2010**, *402*, 2503–2519. [CrossRef]
85. Brans, C.; Dicke, R.H. Mach's Principle and a Relativistic Theory of Gravitation. *Phys. Rev.* **1961**, *124*, 925–935. [CrossRef]
86. Isi, M.; Weinstein, A.J.; Mead, C.; Pitkin, M. Detecting beyond-Einstein polarizations of continuous gravitational waves. *Phys. Rev. D* **2015**, *91*, 082002. [CrossRef]
87. Isi, M.; Pitkin, M.; Weinstein, A.J. Probing dynamical gravity with the polarization of continuous gravitational waves. *Phys. Rev. D* **2017**, *96*, 042001. [CrossRef]
88. Verma, P. Probing Gravitational Waves from Pulsars in Brans–Dicke Theory. *Universe* **2021**, *7*, 235. [CrossRef]
89. Schutz, B.F. Networks of gravitational wave detectors and three figures of merit. *Class. Quantum Gravity* **2011**, *28*, 125023. [CrossRef]
90. Wette, K.; Owen, B.J.; Allen, B.; Ashley, M.; Betzwieser, J.; Christensen, N.; Creighton, T.D.; Dergachev, V.; Gholami, I.; Goetz, E.; et al. Searching for gravitational waves from Cassiopeia A with LIGO. *Class. Quantum Gravity* **2008**, *25*, 235011. [CrossRef]
91. Bildsten, L.; Chakrabarty, D.; Chiu, J.; Finger, M.H.; Koh, D.T.; Nelson, R.W.; Prince, T.A.; Rubin, B.C.; Scott, D.M.; Stollberg, M.; et al. Observations of Accreting Pulsars. *Astrophys. J. Suppl. Ser.* **1997**, *113*, 367–408. [CrossRef]
92. Bertone, G.; Hooper, D. History of dark matter. *Rev. Mod. Phys.* **2018**, *90*, 045002. [CrossRef]
93. Bertone, G.; Croon, D.; Amin, M.; Boddy, K.K.; Kavanagh, B.; Mack, K.J.; Natarajan, P.; Opferkuch, T.; Schutz, K.; Takhistov, V.; et al. Gravitational wave probes of dark matter: Challenges and opportunities. *SciPost Phys. Core* **2020**, *3*, 7. [CrossRef]
94. Arvanitaki, A.; Dimopoulos, S.; Dubovsky, S.; Kaloper, N.; March-Russell, J. String axiverse. *Phys. Rev. D* **2010**, *81*, 123530. [CrossRef]
95. Arvanitaki, A.; Dubovsky, S. Exploring the string axiverse with precision black hole physics. *Phys. Rev. D* **2011**, *83*, 044026. [CrossRef]
96. Brito, R.; Cardoso, V.; Pani, P. *Superradiance*; Lecture Notes in Physics; Springer: Berlin/Heidelberg, Germany, 2020. [CrossRef]
97. Peccei, R.D.; Quinn, H.R. CP Conservation in the Presence of Instantons. *Phys. Rev. Lett.* **1977**, *38*, 1440–1443. [CrossRef]
98. Arvanitaki, A.; Baryakhtar, M.; Huang, X. Discovering the QCD axion with black holes and gravitational waves. *Phys. Rev. D* **2015**, *91*, 084011. [CrossRef]
99. Baryakhtar, M.; Galanis, M.; Lasenby, R.; Simon, O. Black hole superradiance of self-interacting scalar fields. *Phys. Rev. D* **2021**, *103*, 095019. [CrossRef]
100. Palomba, C.; D'Antonio, S.; Astone, P.; Frasca, S.; Intini, G.; La Rosa, I.; Leaci, P.; Mastrogiovanni, S.; Miller, A.; Muciaccia, F.; et al. Direct Constraints on the Ultralight Boson Mass from Searches of Continuous Gravitational Waves. *Phys. Rev. Lett.* **2019**, *123*, 171101. [CrossRef] [PubMed]
101. Zhu, S.J.; Baryakhtar, M.; Papa, M.A.; Tsuna, D.; Kawanaka, N.; Eggenstein, H.B. Characterizing the continuous gravitational-wave signal from boson clouds around Galactic isolated black holes. *Phys. Rev. D* **2020**, *102*, 063020. [CrossRef]

102. Cardoso, V.; Pani, P.; Yu, T.T. Superradiance in rotating stars and pulsar-timing constraints on dark photons. *Phys. Rev. D* **2017**, *95*, 124056. [CrossRef]
103. Day, F.V.; McDonald, J.I. Axion superradiance in rotating neutron stars. *J. Cosmol. Astropart. Phys.* **2019**, *2019*, 051. [CrossRef]
104. Graham, M.; Hearty, C.; Williams, M. Searches for dark photons at accelerators. *arXiv* **2021**, arXiv:2104.10280.
105. Fabbrichesi, M.; Gabrielli, E.; Lanfranchi, G. *The Physics of the Dark Photon*; SpringerBriefs in Physics; Springer: Berlin/Heidelberg, Germany, 2021. [CrossRef]
106. Pierce, A.; Riles, K.; Zhao, Y. Searching for Dark Photon Dark Matter with Gravitational-Wave Detectors. *Phys. Rev. Lett.* **2018**, *121*, 061102. [CrossRef]
107. Graham, P.W.; Kaplan, D.E.; Mardon, J.; Rajendran, S.; Terrano, W.A. Dark matter direct detection with accelerometers. *Phys. Rev. D* **2016**, *93*, 075029. [CrossRef]
108. Carney, D.; Hook, A.; Liu, Z.; Taylor, J.M.; Zhao, Y. Ultralight dark matter detection with mechanical quantum sensors. *New J. Phys.* **2021**, *23*, 023041. [CrossRef]
109. Armaleo, J.M.; López Nacir, D.; Urban, F.R. Searching for spin-2 ULDM with gravitational waves interferometers. *J. Cosmol. Astropart. Phys.* **2021**, *2021*, 053. [CrossRef]
110. Raggi, M.; Kozhuharov, V. Results and perspectives in dark photon physics. *Riv. Nuovo Cim.* **2015**, *38*, 449–505. [CrossRef]
111. Co, R.T.; Hall, L.J.; Harigaya, K. QCD Axion Dark Matter with a Small Decay Constant. *Phys. Rev. Lett.* **2018**, *120*, 211602. [CrossRef] [PubMed]
112. Co, R.T.; Pierce, A.; Zhang, Z.; Zhao, Y. Dark photon dark matter produced by axion oscillations. *Phys. Rev. D* **2019**, *99*, 075002. [CrossRef]
113. Guo, H.K.; Ma, Y.; Shu, J.; Xue, X.; Yuan, Q.; Zhao, Y. Detecting dark photon dark matter with Gaia-like astrometry observations. *J. Cosmol. Astropart. Phys.* **2019**, *2019*, 015. [CrossRef]
114. Xue, X.; Xia, Z.Q.; Zhu, X.; Zhao, Y.; Shu, J.; Yuan, Q.; Bhat, N.D.R.; Cameron, A.D.; Dai, S.; Feng, Y.; et al. High-precision search for dark photon dark matter with the Parkes Pulsar Timing Array. *arXiv* **2021**, arXiv:2112.07687.
115. Arvanitaki, A.; Huang, J.; Van Tilburg, K. Searching for dilaton dark matter with atomic clocks. *Phys. Rev. D* **2015**, *91*, 015015. [CrossRef]
116. Morisaki, S.; Fujita, T.; Michimura, Y.; Nakatsuka, H.; Obata, I. Improved sensitivity of interferometric gravitational-wave detectors to ultralight vector dark matter from the finite light-traveling time. *Phys. Rev. D* **2021**, *103*, L051702. [CrossRef]
117. Guo, H.K.; Riles, K.; Yang, F.W.; Zhao, Y. Searching for dark photon dark matter in LIGO O1 data. *Commun. Phys.* **2019**, *2*, 155. [CrossRef]
118. Michimura, Y.; Fujita, T.; Morisaki, S.; Nakatsuka, H.; Obata, I. Ultralight vector dark matter search with auxiliary length channels of gravitational wave detectors. *Phys. Rev. D* **2020**, *102*, 102001. [CrossRef]
119. Vermeulen, S.M.; Relton, P.; Grote, H.; Raymond, V.; Affeldt, C.; Bergamin, F.; Bisht, A.; Brinkmann, M.; Danzmann, K.; Doravari, S.; et al. Direct limits for scalar field dark matter from a gravitational-wave detector. *Nature* **2021**, *600*, 424–428. [CrossRef]
120. Stadnik, Y.V.; Flambaum, V.V. Enhanced effects of variation of the fundamental constants in laser interferometers and application to dark-matter detection. *Phys. Rev. A* **2016**, *93*, 063630. [CrossRef]
121. Stadnik, Y.V.; Flambaum, V.V. Searching for Dark Matter and Variation of Fundamental Constants with Laser and Maser Interferometry. *Phys. Rev. Lett.* **2015**, *114*, 161301. [CrossRef] [PubMed]
122. Grote, H.; Stadnik, Y.V. Novel signatures of dark matter in laser-interferometric gravitational-wave detectors. *Phys. Rev. Res.* **2019**, *1*, 033187. [CrossRef]
123. Abbott, R.; Abbott, T.D.; Acernese, F.; Ackley, K.; Adams, C.; Adhikari, N.; Adhikari, R.X.; Adya, V.B.; Affeldt, C.; Agarwal, D.; et al. Constraints on dark photon dark matter using data from LIGO's and Virgo's third observing run. *arXiv* **2021**, arXiv:2105.13085.
124. Horowitz, C.; Papa, M.; Reddy, S. Search for compact dark matter objects in the solar system with LIGO data. *Phys. Lett. B* **2020**, *800*, 135072. [CrossRef]
125. Horowitz, C.J.; Widmer-Schnidrig, R. Gravimeter Search for Compact Dark Matter Objects Moving in the Earth. *Phys. Rev. Lett.* **2020**, *124*, 051102. [CrossRef]
126. Carr, B.; Kuhnel, F. Primordial Black Holes as Dark Matter Candidates. *arXiv* **2021**, arXiv:2110.02821.
127. Carr, B.; Kohri, K.; Sendouda, Y.; Yokoyama, J. Constraints on primordial black holes. *Rep. Prog. Phys.* **2021**, *84*, 116902. [CrossRef]
128. Green, A.M.; Kavanagh, B.J. Primordial black holes as a dark matter candidate. *J. Phys. G Nucl. Part. Phys.* **2021**, *48*, 043001. [CrossRef]
129. Carr, B.; Kühnel, F. Primordial Black Holes as Dark Matter: Recent Developments. *Annu. Rev. Nucl. Part. Sci.* **2020**, *70*, 355–394. [CrossRef]
130. Kouvaris, C.; Tinyakov, P.; Tytgat, M.H.G. NonPrimordial Solar Mass Black Holes. *Phys. Rev. Lett.* **2018**, *121*, 221102. [CrossRef]
131. Misner, C.W.; Thorne, K.S.; Wheeler, J.A. *Gravitation*; W. H. Freeman: San Francisco, CA, USA, 1973.
132. Maggiore, M. *Gravitational Waves: Volume 1: Theory and Experiments*; Gravitational Waves; OUP Oxford: Oxford, UK, 2008.
133. Creighton, J.; Anderson, W. Gravitational-Wave Physics and Astronomy: An Introduction to Theory, Experiment and Data Analysis. In *Gravitational-Wave Physics and Astronomy: An Introduction to Theory, Experiment and Data Analysis*; Wiley: Hoboken, NJ, USA, 2011. [CrossRef]
134. Peters, P.C. Gravitational Radiation and the Motion of Two Point Masses. *Phys. Rev.* **1964**, *136*, B1224–B1232. [CrossRef]

135. Tiwari, V.; Klimenko, S.; Necula, V.; Mitselmakher, G. Reconstruction of chirp mass in searches for gravitational wave transients. *Class. Quantum Gravity* **2015**, *33*, 01LT01. [CrossRef]

136. Miller, A.L.; Clesse, S.; De Lillo, F.; Bruno, G.; Depasse, A.; Tanasijczuk, A. Probing planetary-mass primordial black holes with continuous gravitational waves. *Phys. Dark Universe* **2021**, *32*, 100836. [CrossRef]

137. Abbott, R.; Abbott, T.D.; Abraham, S.; Acernese, F.; Ackley, K.; Adams, A.; Adams, C.; Adhikari, R.X.; Adya, V.B.; Affeldt, C.; et al. Gravitational-wave Constraints on the Equatorial Ellipticity of Millisecond Pulsars. *Astrophys. J. Lett.* **2020**, *902*, L21. [CrossRef]

138. Astone, P.; D'Antonio, S.; Frasca, S.; Palomba, C. A method for detection of known sources of continuous gravitational wave signals in non-stationary data. *Class. Quantum Gravity* **2010**, *27*, 194016. [CrossRef]

139. Astone, P.; Colla, A.; D'Antonio, S.; Frasca, S.; Palomba, C. Coherent search of continuous gravitational wave signals: Extension of the 5-vectors method to a network of detectors. *J. Phys. Conf. Ser.* **2012**, *363*, 012038. [CrossRef]

140. Jaranowski, P.; Królak, A.; Schutz, B.F. Data analysis of gravitational-wave signals from spinning neutron stars: The signal and its detection. *Phys. Rev. D* **1998**, *58*, 063001. [CrossRef]

141. Prix, R.; Krishnan, B. Targeted search for continuous gravitational waves: Bayesian versus maximum-likelihood statistics. *Class. Quantum Gravity* **2009**, *26*, 204013. [CrossRef]

142. Prix, R. Search for continuous gravitational waves: Metric of the multidetector $\mathcal{F}$-statistic. *Phys. Rev. D* **2007**, *75*, 023004. [CrossRef]

143. Jaranowski, P.; Królak, A. Searching for gravitational waves from known pulsars using the $\mathcal{F}$ and $\mathcal{G}$ statistics. *Class. Quantum Gravity* **2010**, *27*, 194015. [CrossRef]

144. Cutler, C.; Schutz, B.F. Generalized $\mathcal{F}$-statistic: Multiple detectors and multiple gravitational wave pulsars. *Phys. Rev. D* **2005**, *72*, 063006. [CrossRef]

145. Dupuis, R.J.; Woan, G. Bayesian estimation of pulsar parameters from gravitational wave data. *Phys. Rev. D* **2005**, *72*, 102002. [CrossRef]

146. Pitkin, M.; Isi, M.; Veitch, J.; Woan, G. A nested sampling code for targeted searches for continuous gravitational waves from pulsars. *arXiv* **2017**, arXiv:1705.08978.

147. Piccinni, O.J.; Astone, P.; D'Antonio, S.; Frasca, S.; Intini, G.; Leaci, P.; Mastrogiovanni, S.; Miller, A.; Palomba, C.; Singhal, A. A new data analysis framework for the search of continuous gravitational wave signals. *Class. Quantum Gravity* **2018**, *36*, 015008. [CrossRef]

148. Brady, P.R.; Creighton, T.; Cutler, C.; Schutz, B.F. Searching for periodic sources with LIGO. *Phys. Rev. D* **1998**, *57*, 2101–2116. [CrossRef]

149. Brady, P.R.; Creighton, T. Searching for periodic sources with LIGO. II. Hierarchical searches. *Phys. Rev. D* **2000**, *61*, 082001. [CrossRef]

150. Cutler, C.; Gholami, I.; Krishnan, B. Improved stack-slide searches for gravitational-wave pulsars. *Phys. Rev. D* **2005**, *72*, 042004. [CrossRef]

151. Astone, P.; Colla, A.; D'Antonio, S.; Frasca, S.; Palomba, C. Method for all-sky searches of continuous gravitational wave signals using the frequency-Hough transform. *Phys. Rev. D* **2014**, *90*, 042002. [CrossRef]

152. Palomba, C.; Astone, P.; Frasca, S. Adaptive Hough transform for the search of periodic sources. *Class. Quant. Grav.* **2005**, *22*, S1255–S1264. [CrossRef]

153. Antonucci, F.; Astone, P.; D'Antonio, S.; Frasca, S.; Palomba, C. Detection of periodic gravitational wave sources by Hough transform in the f versus $\dot{f}$ plane. *Class. Quantum Gravity* **2008**, *25*, 184015. [CrossRef]

154. Krishnan, B.; Sintes, A.M.; Papa, M.A.; Schutz, B.F.; Frasca, S.; Palomba, C. Hough transform search for continuous gravitational waves. *Phys. Rev. D* **2004**, *70*, 082001. [CrossRef]

155. Sintes, A.M.; Krishnan, B. Improved Hough search for gravitational wave pulsars. *J. Phys. Conf. Ser.* **2006**, *32*, 206–211. [CrossRef]

156. Jordana, L.S.d.l.; Collaboration, t.L.S.C.a. Hierarchical Hough all-sky search for periodic gravitational waves in LIGO S5 data. *J. Phys. Conf. Ser.* **2010**, *228*, 012004. [CrossRef]

157. Aasi, J.; Abbott, B.P.; Abbott, R.; Abbott, T.; Abernathy, M.R.; Accadia, T.; Acernese, F.; Ackley, K.; Adams, C.; Adams, T.; et al. Implementation of an $\mathcal{F}$-statistic all-sky search for continuous gravitational waves in Virgo VSR1 data. *Class. Quantum Gravity* **2014**, *31*, 165014. [CrossRef]

158. Pisarski, A.; Jaranowski, P. Banks of templates for all-sky narrow-band searches of gravitational waves from spinning neutron stars. *Class. Quantum Gravity* **2015**, *32*, 145014. [CrossRef]

159. Wette, K.; Walsh, S.; Prix, R.; Papa, M. Implementing a semicoherent search for continuous gravitational waves using optimally constructed template banks. *Phys. Rev. D* **2018**, *97*, 123016. [CrossRef]

160. Dergachev, V. Description of PowerFlux Algorithms and Implementation. In *LIGO Document T050186*; 2005. Available online: https://dcc.ligo.org/LIGO-T050186/public (accessed on 2 May 2022).

161. Abbott, R.; Abbott, T.; Abraham, S.; Acernese, F.; Ackley, K.; Adams, A.; Adams, C.; Adhikari, R.; Adya, V.; Affeldt, C.; et al. All-sky search for continuous gravitational waves from isolated neutron stars in the early O3 LIGO data. *Phys. Rev. D* **2021**, *104*, 082004. [CrossRef]

162. Pletsch, H.J. Parameter-space correlations of the optimal statistic for continuous gravitational-wave detection. *Phys. Rev. D* **2008**, *78*, 102005. [CrossRef]

163. Pletsch, H.J.; Allen, B. Exploiting Large-Scale Correlations to Detect Continuous Gravitational Waves. *Phys. Rev. Lett.* **2009**, *103*, 181102. [CrossRef]

164. Pletsch, H.J. Parameter-space metric of semicoherent searches for continuous gravitational waves. *Phys. Rev. D* **2010**, *82*, 042002. [CrossRef]

165. Walsh, S.; Pitkin, M.; Oliver, M.; D'Antonio, S.; Dergachev, V.; Krolak, A.; Astone, P.; Bejger, M.; Di Giovanni, M.; Dorosh, O.; et al. Comparison of methods for the detection of gravitational waves from unknown neutron stars. *Phys. Rev. D* **2016**, *94*, 124010,

166. Dergachev, V. On blind searches for noise dominated signals: A loosely coherent approach. *Class. Quantum Gravity* **2010**, *27*, 205017. [CrossRef]

167. Dergachev, V. Loosely coherent searches for sets of well-modeled signals. *Phys. Rev. D* **2012**, *85*, 062003. [CrossRef]

168. Dergachev, V. Loosely coherent searches for medium scale coherence lengths. *arXiv* **2019**, arXiv:1807.02351.

169. Wette, K.; Dunn, L.; Clearwater, P.; Melatos, A. Deep exploration for continuous gravitational waves at 171–172 Hz in LIGO second observing run data. *Phys. Rev. D* **2021**, *103*, 083020. [CrossRef]

170. Suvorova, S.; Sun, L.; Melatos, A.; Moran, W.; Evans, R. Hidden Markov model tracking of continuous gravitational waves from a neutron star with wandering spin. *Phys. Rev. D* **2016**, *93*, 123009. [CrossRef]

171. Sun, L.; Melatos, A.; Lasky, P.D. Tracking continuous gravitational waves from a neutron star at once and twice the spin frequency with a hidden Markov model. *Phys. Rev. D* **2019**, *99*, 123010. [CrossRef]

172. Sun, L.; Melatos, A.; Suvorova, S.; Moran, W.; Evans, R.J. Hidden Markov model tracking of continuous gravitational waves from young supernova remnants. *Phys. Rev. D* **2018**, *97*, 043013. [CrossRef]

173. D'Antonio, S.; Palomba, C.; Frasca, S.; Astone, P.; La Rosa, I.; Leaci, P.; Mastrogiovanni, S.; Piccinni, O.J.; Pierini, L.; Rei, L. Sidereal filtering: A novel robust method to search for continuous gravitational waves. *Phys. Rev. D* **2021**, *103*, 063030. [CrossRef]

174. Romano, J.D.; Cornish, N.J. Detection methods for stochastic gravitational-wave backgrounds: A unified treatment. *Living Rev. Relativ.* **2017**, *20*, 2. [CrossRef]

175. Thrane, E.; Kandhasamy, S.; Ott, C.D.; Anderson, W.G.; Christensen, N.L.; Coughlin, M.W.; Dorsher, S.; Giampanis, S.; Mandic, V.; Mytidis, A.; et al. Long gravitational-wave transients and associated detection strategies for a network of terrestrial interferometers. *Phys. Rev. D* **2011**, *83*, 083004. [CrossRef]

176. Bayley, J.; Messenger, C.; Woan, G. Generalized application of the Viterbi algorithm to searches for continuous gravitational-wave signals. *Phys. Rev. D* **2019**, *100*, 023006. [CrossRef]

177. Mitra, S.; Dhurandhar, S.; Souradeep, T.; Lazzarini, A.; Mandic, V.; Bose, S.; Ballmer, S. Gravitational wave radiometry: Mapping a stochastic gravitational wave background. *Phys. Rev. D* **2008**, *77*, 042002. [CrossRef]

178. Whelan, J.T.; Sundaresan, S.; Zhang, Y.; Peiris, P. Model-based cross-correlation search for gravitational waves from Scorpius X-1. *Phys. Rev. D* **2015**, *91*, 102005. [CrossRef]

179. Suvorova, S.; Clearwater, P.; Melatos, A.; Sun, L.; Moran, W.; Evans, R. Hidden Markov model tracking of continuous gravitational waves from a binary neutron star with wandering spin. II. Binary orbital phase tracking. *Phys. Rev. D* **2017**, *96*, 102006. [CrossRef]

180. Singhal, A.; Leaci, P.; Astone, P.; D'Antonio, S.; Frasca, S.; Intini, G.; Rosa, I.L.; Mastrogiovanni, S.; Miller, A.; Muciaccia, F.; et al. A resampling algorithm to detect continuous gravitational-wave signals from neutron stars in binary systems. *Class. Quantum Gravity* **2019**, *36*, 205015. [CrossRef]

181. Covas, P.; Sintes, A.M. New method to search for continuous gravitational waves from unknown neutron stars in binary systems. *Phys. Rev. D* **2019**, *99*, 124019. [CrossRef]

182. Goetz, E.; Riles, K. An all-sky search algorithm for continuous gravitational waves from spinning neutron stars in binary systems. *Class. Quantum Gravity* **2011**, *28*, 215006. [CrossRef]

183. Oliver, M.; Keitel, D.; Sintes, A.M. Adaptive transient Hough method for long-duration gravitational wave transients. *Phys. Rev. D* **2019**, *99*, 104067. [CrossRef]

184. Miller, A.; Astone, P.; D'Antonio, S.; Frasca, S.; Intini, G.; La Rosa, I.; Leaci, P.; Mastrogiovanni, S.; Muciaccia, F.; Palomba, C.; et al. Method to search for long duration gravitational wave transients from isolated neutron stars using the generalized frequency-Hough transform. *Phys. Rev. D* **2018**, *98*, 102004. [CrossRef]

185. Prix, R.; Giampanis, S.; Messenger, C. Search method for long-duration gravitational-wave transients from neutron stars. *Phys. Rev. D* **2011**, *84*, 023007. [CrossRef]

186. Sun, L.; Melatos, A. Application of hidden Markov model tracking to the search for long-duration transient gravitational waves from the remnant of the binary neutron star merger GW170817. *Phys. Rev. D* **2019**, *99*, 123003. [CrossRef]

187. Banagiri, S.; Sun, L.; Coughlin, M.W.; Melatos, A. Search strategies for long gravitational-wave transients: Hidden Markov model tracking and seedless clustering. *Phys. Rev. D* **2019**, *100*, 024034. [CrossRef]

188. Keitel, D. Robust semicoherent searches for continuous gravitational waves with noise and signal models including hours to days long transients. *Phys. Rev. D* **2016**, *93*, 084024. [CrossRef]

189. Keitel, D.; Ashton, G. Faster search for long gravitational-wave transients: GPU implementation of the transient $\mathcal{F}$-statistic. *Class. Quantum Gravity* **2018**, *35*, 205003. [CrossRef]

190. Ashton, G.; Prix, R.; Jones, D. A semicoherent glitch-robust continuous-gravitational-wave search method. *Phys. Rev. D* **2018**, *98*, 063011. [CrossRef]

191. Ashton, G.; Prix, R.; Jones, D. Statistical characterization of pulsar glitches and their potential impact on searches for continuous gravitational waves. *Phys. Rev. D* **2017**, *96*, 063004. [CrossRef]

192. Pitkin, M.; Messenger, C.; Fan, X. Hierarchical Bayesian method for detecting continuous gravitational waves from an ensemble of pulsars. *Phys. Rev. D* **2018**, *98*, 063001. [CrossRef]

193. Buono, M.; De Rosa, R.; D'Onofrio, L.; Errico, L.; Palomba, C.; Piccinni, O.J.; Sequino, V. A method for detecting continuous gravitational wave signals from an ensemble of known pulsars. *Class. Quantum Gravity* **2021**, *38*, 135021. [CrossRef]

194. D'Antonio, S.; Palomba, C.; Astone, P.; Frasca, S.; Intini, G.; La Rosa, I.; Leaci, P.; Mastrogiovanni, S.; Miller, A.; Muciaccia, F.; et al. Semicoherent analysis method to search for continuous gravitational waves emitted by ultralight boson clouds around spinning black holes. *Phys. Rev. D* **2018**, *98*, 103017. [CrossRef]

195. Isi, M.; Sun, L.; Brito, R.; Melatos, A. Directed searches for gravitational waves from ultralight bosons. *Phys. Rev. D* **2019**, *99*, 084042. [CrossRef]

196. Miller, A.L.; Astone, P.; Bruno, G.; Clesse, S.; D'Antonio, S.; Depasse, A.; De Lillo, F.; Frasca, S.; La Rosa, I.; Leaci, P.; et al. Probing new light gauge bosons with gravitational-wave interferometers using an adapted semicoherent method. *Phys. Rev. D* **2021**, *103*, 103002. [CrossRef]

197. Morawski, F.; Bejger, M.; Ciecieląg, P. Convolutional neural network classifier for the output of the time-domain $\mathcal{F}$-statistic all-sky search for continuous gravitational waves. *Mach. Learn. Sci. Technol.* **2020**, *1*, 025016. [CrossRef]

198. Yamamoto, T.S.; Tanaka, T. Use of an excess power method and a convolutional neural network in an all-sky search for continuous gravitational waves. *Phys. Rev. D* **2021**, *103*, 084049. [CrossRef]

199. Miller, A.L.; Astone, P.; D'Antonio, S.; Frasca, S.; Intini, G.; La Rosa, I.; Leaci, P.; Mastrogiovanni, S.; Muciaccia, F.; Mitidis, A.; et al. How effective is machine learning to detect long transient gravitational waves from neutron stars in a real search? *Phys. Rev. D* **2019**, *100*, 062005. [CrossRef]

200. Beheshtipour, B.; Papa, M.A. Deep learning for clustering of continuous gravitational wave candidates. *Phys. Rev. D* **2020**, *101*, 064009. [CrossRef]

201. Dreissigacker, C.; Sharma, R.; Messenger, C.; Zhao, R.; Prix, R. Deep-Learning Continuous Gravitational Waves. *Phys. Rev. D* **2019**, *100*, 044009. [CrossRef]

202. Dreissigacker, C.; Prix, R. Deep-Learning Continuous Gravitational Waves: Multiple detectors and realistic noise. *Phys. Rev. D* **2020**, *102*, 022005. [CrossRef]

203. Bayley, J.; Messenger, C.; Woan, G. Robust machine learning algorithm to search for continuous gravitational waves. *Phys. Rev. D* **2020**, *102*, 083024. [CrossRef]

204. Leaci, P. Methods to filter out spurious disturbances in continuous-wave searches from gravitational-wave detectors. *Phys. Scr.* **2015**, *90*, 125001. [CrossRef]

205. Tenorio, R.; Keitel, D.; Sintes, A.M. Application of a hierarchical MCMC follow-up to Advanced LIGO continuous gravitational-wave candidates. *Phys. Rev. D* **2021**, *104*, 084012. [CrossRef]

206. Tenorio, R.; Keitel, D.; Sintes, A.M. Time-frequency track distance for comparing continuous gravitational wave signals. *Phys. Rev. D* **2021**, *103*, 064053. [CrossRef]

207. Intini, G.; Leaci, P.; Astone, P.; Antonio, S.D.; Frasca, S.; Rosa, I.L.; Miller, A.; Palomba, C.; Piccinni, O. A Doppler-modulation based veto to discard false continuous gravitational-wave candidates. *Class. Quantum Gravity* **2020**, *37*, 225007. [CrossRef]

208. Zhu, S.J.; Papa, M.A.; Walsh, S. New veto for continuous gravitational wave searches. *Phys. Rev. D* **2017**, *96*, 124007. [CrossRef]

209. Keitel, D. Distinguishing transient signals and instrumental disturbances in semi-coherent searches for continuous gravitational waves with line-robust statistics. *J. Phys. Conf. Ser.* **2016**, *716*, 012003. [CrossRef]

210. Ashton, G.; Prix, R. Hierarchical multistage MCMC follow-up of continuous gravitational wave candidates. *Phys. Rev. D* **2018**, *97*, 103020. [CrossRef]

211. Isi, M.; Mastrogiovanni, S.; Pitkin, M.; Piccinni, O.J. Establishing the significance of continuous gravitational-wave detections from known pulsars. *Phys. Rev. D* **2020**, *102*, 123027. [CrossRef]

212. Behnke, B.; Papa, M.A.; Prix, R. Postprocessing methods used in the search for continuous gravitational-wave signals from the Galactic Center. *Phys. Rev. D* **2015**, *91*, 064007. [CrossRef]

213. Keitel, D.; Prix, R.; Papa, M.A.; Leaci, P.; Siddiqi, M. Search for continuous gravitational waves: Improving robustness versus instrumental artifacts. *Phys. Rev. D* **2014**, *89*, 064023. [CrossRef]

214. Tenorio, R.; Modafferi, L.M.; Keitel, D.; Sintes, A.M. Empirically estimating the distribution of the loudest candidate from a gravitational-wave search. *arXiv* **2021**, arXiv:2111.12032.

215. Covas, P.; Effler, A.; Goetz, E.; Meyers, P.; Neunzert, A.; Oliver, M.; Pearlstone, B.; Roma, V.; Schofield, R.; Adya, V.; et al. Identification and mitigation of narrow spectral artifacts that degrade searches for persistent gravitational waves in the first two observing runs of Advanced LIGO. *Phys. Rev. D* **2018**, *97*, 082002. [CrossRef]

216. Dreissigacker, C.; Prix, R.; Wette, K. Fast and accurate sensitivity estimation for continuous-gravitational-wave searches. *Phys. Rev. D* **2018**, *98*, 084058. [CrossRef]

217. Dergachev, V. Novel universal statistic for computing upper limits in an ill-behaved background. *Phys. Rev. D* **2013**, *87*, 062001. [CrossRef]

218. Feldman, G.J.; Cousins, R.D. Unified approach to the classical statistical analysis of small signals. *Phys. Rev. D* **1998**, *57*, 3873–3889. [CrossRef]

219. Treves, A.; Turolla, R.; Zane, S.; Colpi, M. Isolated Neutron Stars: Accretors and Coolers. *Publ. Astron. Soc. Pac.* **2000**, *112*, 297–314. [CrossRef]

220. Rajwade, K.; Chennamangalam, J.; Lorimer, D.; Karastergiou, A. The Galactic halo pulsar population. *Mon. Not. R. Astron. Soc.* **2018**, *479*, 3094–3100. [CrossRef]

221. Manchester, R.N.; Hobbs, G.B.; Teoh, A.; Hobbs, M. The Australia Telescope National Facility Pulsar Catalogue. *Astron. J.* **2005**, *129*, 1993–2006. [CrossRef]

222. Abbott, R.; Abe, H.; Acernese, F.; Ackley, K.; Adhikari, N.; Adhikari, R.X.; Adkins, V.K.; Adya, V.B.; Affeldt, C.; Agarwal, D.; et al. Searches for Gravitational Waves from Known Pulsars at Two Harmonics in the Second and Third LIGO-Virgo Observing Runs. *arXiv* **2021**, arXiv:2111.13106.

223. Pitkin, M.; Gill, C.; Jones, D.I.; Woan, G.; Davies, G.S. First results and future prospects for dual-harmonic searches for gravitational waves from spinning neutron stars. *Mon. Not. R. Astron. Soc.* **2015**, *453*, 4399–4420. [CrossRef]

224. Abbott, B.P.; Abbott, R.; Abbott, T.D.; Abraham, S.; Acernese, F.; Ackley, K.; Adams, C.; Adhikari, R.X.; Adya, V.B.; Affeldt, C.; et al. Searches for Gravitational Waves from Known Pulsars at Two Harmonics in 2015–2017 LIGO Data. *Astrophys. J.* **2019**, *879*, 10. [CrossRef]

225. Abbott, B.P.; Abbott, R.; Abbott, T.D.; Abernathy, M.R.; Acernese, F.; Ackley, K.; Adams, C.; Adams, T.; Addesso, P.; Adhikari, R.X.; et al. First Search for Gravitational Waves from Known Pulsars with Advanced LIGO. *Astrophys. J.* **2017**, *839*, 12. [CrossRef]

226. Abbott, B.P.; et al. First Search for Nontensorial Gravitational Waves from Known Pulsars. *Phys. Rev. Lett.* **2018**, *120*, 031104. [CrossRef] [PubMed]

227. Abbott, R.; Abbott, T.D.; Abraham, S.; Acernese, F.; Ackley, K.; Adams, A.; Adams, C.; Adhikari, R.X.; Adya, V.B.; Affeldt, C.; et al. Diving below the Spin-down Limit: Constraints on Gravitational Waves from the Energetic Young Pulsar PSR J0537-6910. *Astrophys. J. Lett.* **2021**, *913*, L27. [CrossRef]

228. Ho, W.C.G.; Espinoza, C.M.; Arzoumanian, Z.; Enoto, T.; Tamba, T.; Antonopoulou, D.; Bejger, M.; Guillot, S.; Haskell, B.; Ray, P.S. Return of the Big Glitcher: NICER timing and glitches of PSR J0537-6910. *Mon. Not. R. Astron. Soc.* **2020**, *498*, 4605–4614. [CrossRef] [PubMed]

229. Abbott, R.; Abbott, T.D.; Abraham, S.; Acernese, F.; Ackley, K.; Adams, A.; Adams, C.; Adhikari, R.X.; Adya, V.B.; Affeldt, C.; et al. Constraints from LIGO O3 Data on Gravitational-wave Emission Due to R-modes in the Glitching Pulsar PSR J0537–6910. *Astrophys. J.* **2021**, *922*, 71. [CrossRef]

230. Fesik, L.; Papa, M.A. First Search for r-mode Gravitational Waves from PSR J0537-6910. *Astrophys. J.* **2020**, *895*, 11. [CrossRef]

231. Andersson, N.; Antonopoulou, D.; Espinoza, C.M.; Haskell, B.; Ho, W.C.G. The Enigmatic Spin Evolution of PSR J0537–6910: R-modes, Gravitational Waves, and the Case for Continued Timing. *Astrophys. J.* **2018**, *864*, 137. [CrossRef]

232. Antonopoulou, D.; Espinoza, C.M.; Kuiper, L.; Andersson, N. Pulsar spin-down: The glitch-dominated rotation of PSR J0537-6910. *Mon. Not. R. Astron. Soc.* **2017**, *473*, 1644–1655. [CrossRef]

233. Rajbhandari, B.; Owen, B.J.; Caride, S.; Inta, R. First searches for gravitational waves from r-modes of the Crab pulsar. *Phys. Rev. D* **2021**, *104*, 122008. [CrossRef]

234. Mastrogiovanni, S.; Astone, P.; D'Antonio, S.; Frasca, S.; Intini, G.; Leaci, P.; Miller, A.; Palomba, C.; Piccinni, O.J.; Singhal, A. An improved algorithm for narrow-band searches of continuous gravitational waves. *Class. Quantum Gravity* **2017**, *34*, 135007. [CrossRef]

235. Astone, P.; Colla, A.; D'Antonio, S.; Frasca, S.; Palomba, C.; Serafinelli, R. Method for narrow-band search of continuous gravitational wave signals. *Phys. Rev. D* **2014**, *89*, 062008. [CrossRef]

236. Ashok, A.; Beheshtipour, B.; Papa, M.A.; Freire, P.C.C.; Steltner, B.; Machenschalk, B.; Behnke, O.; Allen, B.; Prix, R. New Searches for Continuous Gravitational Waves from Seven Fast Pulsars. *Astrophys. J.* **2021**, *923*, 85. [CrossRef]

237. Nieder, L.; Clark, C.J.; Bassa, C.G.; Wu, J.; Singh, A.; Donner, J.Y.; Allen, B.; Breton, R.P.; Dhillon, V.S.; Eggenstein, H.B.; et al. Detection and Timing of Gamma-Ray Pulsations from the 707 Hz Pulsar J0952-0607. *Astrophys. J.* **2019**, *883*, 42. [CrossRef]

238. Nieder, L.; Clark, C.J.; Kandel, D.; Romani, R.W.; Bassa, C.G.; Allen, B.; Ashok, A.; Cognard, I.; Fehrmann, H.; Freire, P.; et al. Discovery of a Gamma-Ray Black Widow Pulsar by GPU-accelerated Einstein@Home. *Astrophys. J. Lett.* **2020**, *902*, L46. [CrossRef]

239. Beniwal, D.; Clearwater, P.; Dunn, L.; Melatos, A.; Ottaway, D. Search for continuous gravitational waves from ten H.E.S.S. sources using a hidden Markov model. *Phys. Rev. D* **2021**, *103*, 083009. [CrossRef]

240. Abbott, R.; Abbott, T.D.; Acernese, F.; Ackley, K.; Adams, C.; Adhikari, N.; Adhikari, R.X.; Adya, V.B.; Affeldt, C.; Agarwal, D.; et al. Narrowband searches for continuous and long-duration transient gravitational waves from known pulsars in the LIGO-Virgo third observing run. *arXiv* **2021**, arXiv:2112.10990.

241. Modafferi, L.M.; Moragues, J.; Keitel, D.; Collaboration, L.S.; Collaboration, V.; Collaboration, K. Search setup for long-duration transient gravitational waves from glitching pulsars during LIGO-Virgo third observing run. *arXiv* **2022**, arXiv:2201.08785.

242. Keitel, D.; Woan, G.; Pitkin, M.; Schumacher, C.; Pearlstone, B.; Riles, K.; Lyne, A.G.; Palfreyman, J.; Stappers, B.; Weltevrede, P. First search for long-duration transient gravitational waves after glitches in the Vela and Crab pulsars. *Phys. Rev. D* **2019**, *100*, 064058. [CrossRef]

243. Abbott, B.; Abbott, R.; Abbott, T.; Abraham, S.; Acernese, F.; Ackley, K.; Adams, C.; Adhikari, R.; Adya, V.; Affeldt, C.; et al. Narrow-band search for gravitational waves from known pulsars using the second LIGO observing run. *Phys. Rev. D* **2019**, *99*, 122002. [CrossRef]

244. Abbott, B.; Abbott, R.; Abbott, T.; Acernese, F.; Ackley, K.; Adams, C.; Adams, T.; Addesso, P.; Adhikari, R.; Adya, V.; et al. First narrow-band search for continuous gravitational waves from known pulsars in advanced detector data. *Phys. Rev. D* **2017**, *96*, 122006. [CrossRef]

245. Ming, J.; Krishnan, B.; Papa, M.A.; Aulbert, C.; Fehrmann, H. Optimal directed searches for continuous gravitational waves. *Phys. Rev. D* **2016**, *93*, 064011. [CrossRef]
246. Ming, J.; Papa, M.A.; Krishnan, B.; Prix, R.; Beer, C.; Zhu, S.J.; Eggenstein, H.B.; Bock, O.; Machenschalk, B. Optimally setting up directed searches for continuous gravitational waves in Advanced LIGO O1 data. *Phys. Rev. D* **2018**, *97*, 024051. [CrossRef]
247. Abbott, R.; Abbott, T.D.; Acernese, F.; Ackley, K.; Adams, C.; Adhikari, N.; Adhikari, R.X.; Adya, V.B.; Affeldt, C.; Agarwal, D.; et al. Search of the Early O3 LIGO Data for Continuous Gravitational Waves from the Cassiopeia A and Vela Jr. Supernova Remnants. *arXiv* **2021**, arXiv:2111.15116.
248. Abbott, R.; Abbott, T.D.; Abraham, S.; Acernese, F.; Ackley, K.; Adams, A.; Adams, C.; Adhikari, R.X.; Adya, V.B.; Affeldt, C.; et al. Searches for Continuous Gravitational Waves from Young Supernova Remnants in the Early Third Observing Run of Advanced LIGO and Virgo. *Astrophys. J.* **2021**, *921*, 80. [CrossRef]
249. Papa, M.A.; Ming, J.; Gotthelf, E.V.; Allen, B.; Prix, R.; Dergachev, V.; Eggenstein, H.B.; Singh, A.; Zhu, S.J. Search for Continuous Gravitational Waves from the Central Compact Objects in Supernova Remnants Cassiopeia A, Vela Jr., and G347.3–0.5. *Astrophys. J.* **2020**, *897*, 22. [CrossRef]
250. Ming, J.; Papa, M.A.; Singh, A.; Eggenstein, H.B.; Zhu, S.J.; Dergachev, V.; Hu, Y.; Prix, R.; Machenschalk, B.; Beer, C.; et al. Results from an Einstein@Home search for continuous gravitational waves from Cassiopeia A, Vela Jr., and G347.3. *Phys. Rev. D* **2019**, *100*, 024063. [CrossRef]
251. Ming, J.; Papa, M.A.; Eggenstein, H.B.; Machenschalk, B.; Steltner, B.; Prix, R.; Allen, B.; Behnke, O. Results From an Einstein@Home Search for Continuous Gravitational Waves From G347.3 at Low Frequencies in LIGO O2 Data. *Astrophys. J.* **2022**, *925*, 8. [CrossRef]
252. Lindblom, L.; Owen, B.J. Directed searches for continuous gravitational waves from twelve supernova remnants in data from Advanced LIGO's second observing run. *Phys. Rev. D* **2020**, *101*, 083023. [CrossRef]
253. Millhouse, M.; Strang, L.; Melatos, A. Search for gravitational waves from 12 young supernova remnants with a hidden Markov model in Advanced LIGO's second observing run. *Phys. Rev. D* **2020**, *102*, 083025. [CrossRef]
254. Abbott, B.P.; Abbott, R.; Abbott, T.D.; Abraham, S.; Acernese, F.; Ackley, K.; Adams, C.; Adhikari, R.X.; Adya, V.B.; Affeldt, C.; et al. Searches for Continuous Gravitational Waves from 15 Supernova Remnants and Fomalhaut b with Advanced LIGO. *Astrophys. J.* **2019**, *875*, 122. [CrossRef]
255. Jones, D.; Sun, L. Search for continuous gravitational waves from Fomalhaut b in the second Advanced LIGO observing run with a hidden Markov model. *Phys. Rev. D* **2021**, *103*, 023020. [CrossRef]
256. Abbott, R.; Abbott, T.; Acernese, F.; Ackley, K.; Adams, C.; Adhikari, N.; Adhikari, R.; Adya, V.; Affeldt, C.; Agarwal, D.; et al. Search for continuous gravitational waves from 20 accreting millisecond x-ray pulsars in O3 LIGO data. *Phys. Rev. D* **2022**, *105*, 022002. [CrossRef]
257. Middleton, H.; Clearwater, P.; Melatos, A.; Dunn, L. Search for gravitational waves from five low mass x-ray binaries in the second Advanced LIGO observing run with an improved hidden Markov model. *Phys. Rev. D* **2020**, *102*, 023006. [CrossRef]
258. Haskell, B.; Patruno, A. Are Gravitational Waves Spinning Down PSR J1023 + 0038? *Phys. Rev. Lett.* **2017**, *119*, 161103. [CrossRef]
259. Zhang, Y.; Papa, M.A.; Krishnan, B.; Watts, A.L. Search for Continuous Gravitational Waves from Scorpius X-1 in LIGO O2 Data. *Astrophys. J. Lett.* **2021**, *906*, L14. [CrossRef]
260. Abbott, B.; Abbott, R.; Abbott, T.; Acernese, F.; Ackley, K.; Adams, C.; Adams, T.; Addesso, P.; Adhikari, R.; Adya, V.; et al. Search for gravitational waves from Scorpius X-1 in the first Advanced LIGO observing run with a hidden Markov model. *Phys. Rev. D* **2017**, *95*, 122003. [CrossRef]
261. Abbott, B.; Abbott, R.; Abbott, T.; Abraham, S.; Acernese, F.; Ackley, K.; Adams, C.; Adhikari, R.; Adya, V.; Affeldt, C.; et al. Search for gravitational waves from Scorpius X-1 in the second Advanced LIGO observing run with an improved hidden Markov model. *Phys. Rev. D* **2019**, *100*, 122002. [CrossRef]
262. Abbott, B.P.; Abbott, R.; Abbott, T.D.; Acernese, F.; Ackley, K.; Adams, C.; Adams, T.; Addesso, P.; Adhikari, R.X.; Adya, V.B.; et al. Upper Limits on Gravitational Waves from Scorpius X-1 from a Model-based Cross-correlation Search in Advanced LIGO Data. *Astrophys. J.* **2017**, *847*, 47. [CrossRef]
263. Abbott, R.; Abbott, T.D.; Acernese, F.; Ackley, K.; Adams, C.; Adhikari, N.; Adhikari, R.X.; Adya, V.B.; Affeldt, C.; Agarwal, D.; et al. Search for gravitational waves from Scorpius X-1 with a hidden Markov model in O3 LIGO data. *arXiv* **2022**, arXiv:2201.10104.
264. Bildsten, L. Gravitational Radiation and Rotation of Accreting Neutron Stars. *Astrophys. J.* **1998**, *501*, L89–L93. [CrossRef]
265. Wagoner, R.V. Gravitational radiation from accreting neutron stars. *Astrophys. J.* **1984**, *278*, 345–348. [CrossRef]
266. Wang, L.; Steeghs, D.; Galloway, D.K.; Marsh, T.; Casares, J. Precision Ephemerides for Gravitational-wave Searches—III. Revised system parameters of Sco X-1. *Mon. Not. R. Astron. Soc.* **2018**, *478*, 5174–5183. [CrossRef]
267. Meadors, G.D.; Krishnan, B.; Papa, M.A.; Whelan, J.T.; Zhang, Y. Resampling to accelerate cross-correlation searches for continuous gravitational waves from binary systems. *Phys. Rev. D* **2018**, *97*, 044017. [CrossRef]
268. Fomalont, E.B.; Geldzahler, B.J.; Bradshaw, C.F. Scorpius X-1: The Evolution and Nature of the Twin Compact Radio Lobes. *Astrophys. J.* **2001**, *558*, 283–301. [CrossRef]
269. Abbott, R.; Abbott, T.; Abraham, S.; Acernese, F.; Ackley, K.; Adams, A.; Adams, C.; Adhikari, R.; Adya, V.; Affeldt, C.; et al. Search for anisotropic gravitational-wave backgrounds using data from Advanced LIGO and Advanced Virgo's first three observing runs. *Phys. Rev. D* **2021**, *104*, 022005. [CrossRef]

270. Abbott, R.; Abbott, T.D.; Acernese, F.; Ackley, K.; Adams, C.; Adhikari, N.; Adhikari, R.X.; Adya, V.B.; Affeldt, C.; Agarwal, D.; et al. All-sky search for continuous gravitational waves from isolated neutron stars using Advanced LIGO and Advanced Virgo O3 data. *arXiv* **2022**, arXiv:2201.00697.

271. Miller, A.L.; Aggarwal, N.; Clesse, S.; Lillo, F.D. Constraints on planetary and asteroid-mass primordial black holes from continuous gravitational-wave searches. *arXiv* **2021**, arXiv:2110.06188.

272. Dergachev, V.; Papa, M.A. Results from the First All-Sky Search for Continuous Gravitational Waves from Small-Ellipticity Sources. *Phys. Rev. Lett.* **2020**, *125*, 171101. [CrossRef]

273. Dergachev, V.; Papa, M.A. Results from high-frequency all-sky search for continuous gravitational waves from small-ellipticity sources. *Phys. Rev. D* **2021**, *103*, 063019. [CrossRef]

274. Dergachev, V.; Papa, M.A. Search for continuous gravitational waves from small-ellipticity sources at low frequencies. *Phys. Rev. D* **2021**, *104*, 043003. [CrossRef]

275. Steltner, B.; Papa, M.A.; Eggenstein, H.B.; Allen, B.; Dergachev, V.; Prix, R.; Machenschalk, B.; Walsh, S.; Zhu, S.J.; Behnke, O.; et al. Einstein@Home All-sky Search for Continuous Gravitational Waves in LIGO O2 Public Data. *Astrophys. J.* **2021**, *909*, 79. [CrossRef]

276. Abbott, B.; Abbott, R.; Abbott, T.; Abraham, S.; Acernese, F.; Ackley, K.; Adams, C.; Adhikari, R.; Adya, V.; Affeldt, C.; et al. All-sky search for continuous gravitational waves from isolated neutron stars using Advanced LIGO O2 data. *Phys. Rev. D* **2019**, *100*, 024004. [CrossRef]

277. Dergachev, V.; Papa, M.A. Results from an extended Falcon all-sky survey for continuous gravitational waves. *Phys. Rev. D* **2020**, *101*, 022001. [CrossRef]

278. Dergachev, V.; Papa, M.A. Sensitivity Improvements in the Search for Periodic Gravitational Waves Using O1 LIGO Data. *Phys. Rev. Lett.* **2019**, *123*, 101101. [CrossRef]

279. Abbott, B.; Abbott, R.; Abbott, T.; Acernese, F.; Ackley, K.; Adams, C.; Adams, T.; Addesso, P.; Adhikari, R.; Adya, V.; et al. First low-frequency Einstein@Home all-sky search for continuous gravitational waves in Advanced LIGO data. *Phys. Rev. D* **2017**, *96*, 122004. [CrossRef]

280. Abbott, R.; Abbott, T.E.A. All-sky search in early O3 LIGO data for continuous gravitational-wave signals from unknown neutron stars in binary systems. *Phys. Rev. D* **2021**, *103*, 064017. [CrossRef]

281. Tenorio, R.; The LIGO Scientific Collaboration; Virgo Collaboration. An all-sky search in early O3 LIGO data for continuous gravitational-wave signals from unknown neutron stars in binary systems. *arXiv* **2021**, arXiv:2105.07455.

282. Covas, P.; Sintes, A.M. First All-Sky Search for Continuous Gravitational-Wave Signals from Unknown Neutron Stars in Binary Systems Using Advanced LIGO Data. *Phys. Rev. Lett.* **2020**, *124*, 191102. [CrossRef]

283. Singh, A.; Papa, M.A.; Dergachev, V. Characterizing the sensitivity of isolated continuous gravitational wave searches to binary orbits. *Phys. Rev. D* **2019**, *100*, 024058. [CrossRef]

284. Rajwade, K.M.; Lorimer, D.R.; Anderson, L.D. Detecting Pulsars in the Galactic Centre. *Mon. Not. R. Astron. Soc.* **2017**, *471*, 730–739. Available online: https://academic.oup.com/mnras/article-pdf/471/1/730/19376227/stx1661.pdf (accessed on 2 May 2022). [CrossRef]

285. Kim, C.; Davies, M.B. Neutron Stars in the Galactic Center. *J. Korean Astron. Soc.* **2018**, *51*, 165–170. [CrossRef]

286. Ajello, M.; Albert, A.; Atwood, W.B.; Barbiellini, G.; Bastieri, D.; Bechtol, K.; Bellazzini, R.; Bissaldi, E.; Blandford, R.D.; Bloom, E.D.; et al. Fermi-lat observations of high-energy γ-ray emission toward the galactic center. *Astrophys. J.* **2016**, *819*, 44. [CrossRef]

287. Di Mauro, M. Characteristics of the Galactic Center excess measured with 11 years of Fermi -LAT data. *Phys. Rev. D* **2021**, *103*, 063029. [CrossRef]

288. collaboration, H. Acceleration of petaelectronvolt protons in the Galactic Centre. *Nature* **2016**, *531*, 476–479. [CrossRef]

289. Bartels, R.; Krishnamurthy, S.; Weniger, C. Strong Support for the Millisecond Pulsar Origin of the Galactic Center GeV Excess. *Phys. Rev. Lett.* **2016**, *116*, 051102. [CrossRef]

290. Calore, F.; Mauro, M.D.; Donato, F.; Hessels, J.W.T.; Weniger, C. Radio detection prospects for a bulge population of millisecond pulsars as suggested by fermi-lat observations of the inner galaxy. *Astrophys. J.* **2016**, *827*, 143. [CrossRef]

291. Grégoire, T..; Knödlseder, J. Constraining the Galactic millisecond pulsar population using Fermi Large Area Telescope. *Astron. Astrophys.* **2013**, *554*, A62. [CrossRef]

292. Hooper, D.; Linden, T. Millisecond pulsars, TeV halos, and implications for the Galactic Center gamma-ray excess. *Phys. Rev. D* **2018**, *98*, 043005. [CrossRef]

293. Buschmann, M.; Rodd, N.L.; Safdi, B.R.; Chang, L.J.; Mishra-Sharma, S.; Lisanti, M.; Macias, O. Foreground mismodeling and the point source explanation of the Fermi Galactic Center excess. *Phys. Rev. D* **2020**, *102*, 023023. [CrossRef]

294. Abbott, R.; Abbott, T.D.; Acernese, F.; Ackley, K.; Adams, C.; Adhikari, N.; Adhikari, R.X.; Adya, V.B.; Affeldt, C.; Agarwal, D.; et al. Search for continuous gravitational wave emission from the Milky Way center in O3 LIGO–Virgo data. *arXiv* **2022**, arXiv:2204.04523.

295. Piccinni, O.J.; Astone, P.; D'Antonio, S.; Frasca, S.; Intini, G.; La Rosa, I.; Leaci, P.; Mastrogiovanni, S.; Miller, A.; Palomba, C. Directed search for continuous gravitational-wave signals from the Galactic Center in the Advanced LIGO second observing run. *Phys. Rev. D* **2020**, *101*, 082004. [CrossRef]

296. Dergachev, V.; Papa, M.A.; Steltner, B.; Eggenstein, H.B. Loosely coherent search in LIGO O1 data for continuous gravitational waves from Terzan 5 and the Galactic Center. *Phys. Rev. D* **2019**, *99*, 084048. [CrossRef]

297. Abbott, R.; Abbott, T.D.; Acernese, F.; Ackley, K.; Adams, C.; Adhikari, N.; Adhikari, R.X.; Adya, V.B.; Affeldt, C.; Agarwal, D.; et al. All-sky search for gravitational wave emission from scalar boson clouds around spinning black holes in LIGO O3 data. *arXiv* **2021**, arXiv:2111.15507.

298. Sun, L.; Brito, R.; Isi, M. Search for ultralight bosons in Cygnus X-1 with Advanced LIGO. *Phys. Rev. D* **2020**, *101*, 063020. [CrossRef]

299. Schlamminger, S.; Choi, K.Y.; Wagner, T.A.; Gundlach, J.H.; Adelberger, E.G. Test of the Equivalence Principle Using a Rotating Torsion Balance. *Phys. Rev. Lett.* **2008**, *100*, 041101. [CrossRef]

300. Bergé, J.; Brax, P.; Métris, G.; Pernot-Borràs, M.; Touboul, P.; Uzan, J.P. MICROSCOPE Mission: First Constraints on the Violation of the Weak Equivalence Principle by a Light Scalar Dilaton. *Phys. Rev. Lett.* **2018**, *120*, 141101. [CrossRef]

301. Punturo, M.; Abernathy, M.; Acernese, F.; Allen, B.; Andersson, N.; Arun, K.; Barone, F.; Barr, B.; Barsuglia, M.; Beker, M.; et al. The Einstein Telescope: A third-generation gravitational wave observatory. *Class. Quantum Gravity* **2010**, *27*, 194002. [CrossRef]

302. Reitze, D.; Adhikari, R.X.; Ballmer, S.; Barish, B.; Barsotti, L.; Billingsley, G.; Brown, D.A.; Chen, Y.; Coyne, D.; Eisenstein, R.; et al. Cosmic Explorer: The U.S. Contribution to Gravitational-Wave Astronomy beyond LIGO. *arXiv* **2019**, arXiv:1907.04833.

303. Danzmann, K.; The LISA Pathfinder Team.; The eLISA Consortium. LISA and its pathfinder. *Nat. Phys.* **2015**, *11*, 613–615. [CrossRef]

304. Kalogera, V.; Sathyaprakash, B.S.; Bailes, M.; Bizouard, M.A.; Buonanno, A.; Burrows, A.; Colpi, M.; Evans, M.; Fairhurst, S.; Hild, S.; Kasliwal, M.M.; et al. The Next Generation Global Gravitational Wave Observatory: The Science Book. *arXiv* **2021**, arXiv:2111.06990.

305. Kawamura, S.; Ando, M.; Seto, N.; Sato, S.; Musha, M.; Kawano, I.; Yokoyama, J.I.; Tanaka, T.; Ioka, K.; Akutsu, T.; Takashima, T.; et al. Current status of space gravitational wave antenna DECIGO and B-DECIGO. *arXiv* **2020**, arXiv:2006.13545.

306. Luo, J.; Chen, L.S.; Duan, H.Z.; Gong, Y.G.; Hu, S.; Ji, J.; Liu, Q.; Mei, J.; Milyukov, V.; Sazhin, M.; et al. TianQin: A space-borne gravitational wave detector. *Class. Quantum Gravity* **2016**, *33*, 035010. [CrossRef]